



**BRNO UNIVERSITY OF TECHNOLOGY**  
VYSOKÉ UČENÍ TECHNICKÉ V BRNĚ

**FACULTY OF INFORMATION TECHNOLOGY**  
FAKULTA INFORMAČNÍCH TECHNOLOGIÍ

**DEPARTMENT OF COMPUTER GRAPHICS AND MULTIMEDIA**  
ÚSTAV POČÍTAČOVÉ GRAFIKY A MULTIMÉDIÍ

**LUNAR LANDING SIMULATION**  
SIMULACE PŘISTÁNÍ SONDY NA MĚSÍCI

**BACHELOR'S THESIS**  
BAKALÁŘSKÁ PRÁCE

**AUTHOR**  
AUTOR PRÁCE

**ERIKA DO**

**SUPERVISOR**  
VEDOUCÍ PRÁCE

**doc. Ing. PETER CHUDÝ, Ph.D., MBA**

**BRNO 2024**

# Bachelor's Thesis Assignment



Institut: Department of Computer Graphics and Multimedia (DCGM)  
Student: **Do Erika**  
Programme: Information Technology  
Title: **Lunar Landing Simulation**  
Category: Modelling and Simulation  
Academic year: 2023/24

154981

Assignment:

1. Research lunar landing problem and descent trajectory physics.
2. Perform computation of optimal descent trajectory.
3. Design and implement visualization environment, for which you create or download from relevant sources basic 3D models and 3D engine for descent maneuver interpretation.
4. Evaluate achieved results and discuss potential further improvements.

Literature:

- Bonnans, F., Martinon, P., Giorgi, D., Gréard, V., Maindrault, S. et al. BOCOP 2.2.0 - User Guide [online]. Available at: <https://files.inria.fr/bocop/UserGuide-BOCOP.pdf>.
- Hawkins, A. M. Constrained Trajectory Optimization of a Soft Lunar Landing from a Parking Orbit. Cambridge, 2005. Masters Thesis. Massachusetts Institute of Technology. Dept. of Aeronautics and Astronautics. Available at: <https://dspace.mit.edu/handle/1721.1/32431>.
- Ulrich W., Astronautics, The Physics of Space Flight. Springer Verlag. third edition. 2019. ISBN 978-3-319-74372-1.

Requirements for the semestral defence:

Tasks 1, 2 and partially task 3.

Detailed formal requirements can be found at <https://www.fit.vut.cz/study/theses/>

Supervisor: **Chudý Peter, doc. Ing., Ph.D., MBA**  
Head of Department: Černocký Jan, prof. Dr. Ing.  
Beginning of work: 1.11.2023  
Submission deadline: 31.7.2024  
Approval date: 9.11.2023

## Abstract

The objective of this bachelor's thesis was to compute and visually represent the optimal lunar descent trajectory for the Chandrayaan-3 spacecraft. This was achieved through the utilisation of Bocop, an optimal control problem solver, while the environment was constructed using GDScript with the assistance of the 3D engine Godot. The measured coordinates were sourced from ISRO, the national space agency of India. Subsequently, the optimal descent trajectory was calculated and compared against the actual data acquired from Chandrayaan-3's lunar landing. The resulting application provides users with the ability to intuitively visualise the optimal descent trajectory.

## Abstrakt

Cílem této bakalářské práce bylo vypočítat a vizuálně znázornit optimální trajektorii sestupu na Měsíc pro kosmickou loď Chandrayaan-3. Toho bylo dosaženo využitím Bocop, jež řeší problémy optimálního řízení, zatímco prostředí bylo vytvořeno v jazyce GDScript s pomocí 3D enginu Godot. Naměřené souřadnice byly získány od ISRO, státní indické vesmírné agentury. Následně byla spočítána optimální sestupová trajektorie a porovnána se skutečnými daty, získanými z přistání na Měsici mise Chandrayaan-3. Výsledná aplikace dává uživatelům možnost si intuitivně zobrazit optimální sestupovou trajektorii.

## Keywords

Chandrayaan-3, lunar landing, simulation, optimal descent trajectory, optimal control, Bocop, Godot Engine

## Klíčová slova

Chandrayaan-3, přistání na Měsici, simulace, optimální trajektorie sestupu, optimální řízení, Bocop, Godot Engine

## Reference

DO, Erika. *LUNAR LANDING SIMULATION*. Brno, 2024. Bachelor's thesis. Brno University of Technology, Faculty of Information Technology. Supervisor doc. Ing. Peter Chudý, Ph.D., MBA

# Rozšířený abstrakt

Do konce roku 2022 se pouze tři státy světa pyšnily úspěšným přistáním na Měsíci: Rusko, USA, Čína. Navíc Spojené státy americké jsou první (a nadále jedinou) zemí, která dokázala vyslat vesmírnou loď s posádkou na Měsíc a zase zpátky. Spousta dalších kosmických organizací se zoufale snažilo připojit k této trojici států, avšak delší dobu bez úspěchu. Vše se změnilo 6. července 2023, když státní indická vesmírná agentura, ISRO, oznámila datum počátku mise Chandrayaan-3. Jednalo se o třetí misi v pořadí, jejíž primárním úkolem bylo pokračovat tam, kde předešlá mise Chandrayaan-2 selhala, a tím byl závěrečný sestup k povrchu Měsíce.

Tato bakalářské práce se zabývá výpočtem optimální trajektorie přistání na Měsíci pro kosmickou loď Chandrayaan-3 a vizualizací sestupového manévrování v 3D prostředí.

V první části byla provedena analýza mise Chandrayaan-3 a jejích předchůdců. To rovněž obnášelo zjištění klíčových údajů, bez kterých bychom se v této práci neobešli. Technické parametry lodi byly získány z oficiálních stránek ISRO. Informace o astronomických tělesech byly opatřeny z veřejně dostupných zdrojů na internetu. Je nutné podotknout, že přistávací manévr byl zjednodušen na pohyb v jedné rovině se třemi stupni volnosti, což výrazně usnadnilo výpočty. K dalším nezbytnostem patřilo definování dvou vztažných polárních souřadných soustav: první byla inerciální se středem v těžišti Měsíce, druhá naopak rotující se středem v těžisti vesmírné lodi. V neposlední řadě byly odvozeny potřebné pohybové rovnice, vycházející z Newtonovy klasické mechaniky.

Výpočet optimální trajektorie byl modelován jako problém optimálního řízení. To zahrnovalo možnost měnit trajektorii v čase pomocí řídicích prvků, tj. tah motoru a úhlové zrychlení, způsobeného systémem řízení náklonu. Naším cílem bylo maximalizovat finální hmotnost přistávacího modulu, což posloužilo jako užitková funkce. Problém byl implementován v softwarovém nástroji Bocop<sup>1</sup>, který je na jejich řešení specializovaný. Před samotným výpočtem bylo zapotřebí stanovit stavový a řídicí vektor, meze jednotlivých veličin, počáteční a koncové podmínky, konstanty, pohybové rovnice a také již zmiňovanou užitkovou funkci. Výsledná optimální trajektorie splnila všechny omezující požadavky, a zbylá hmotnost paliva byla vyšší než-li po přistání u reálné lodi Chandrayaan-3.

V druhé části práce bylo vyvinuto vizualizační prostředí v jazyce GDScript s použitím 3D enginu Godot<sup>2</sup>, jehož síla spočívá v produkci kvalitních 2D a 3D aplikací. Vytvořený program se načte s již zabudovanou vypočítanou trajektorií a následně spustí animaci sestupu kosmické lodi Chandrayaan-3 po dané trase. Do vizualizace lze volně zasahovat a měnit parametry jako je čas, rychlosť přehrání či úhel kamery.

---

<sup>1</sup><http://www.bocop.org/>

<sup>2</sup><https://godotengine.org/>

# LUNAR LANDING SIMULATION

## Declaration

I hereby declare that this Bachelor's thesis was prepared as an original work by the author under the supervision of Mr. doc. Ing. Peter Chudý, Ph.D., MBA. I have listed all the literary sources, publications and other sources, which were used during the preparation of this thesis.

.....  
Erika Do  
July 31, 2024

## Acknowledgements

I would like to extend my sincere thanks to supervisor doc. Ing. Peter Chudý, Ph.D., MBA for the guidance and prompt feedback throughout this process. I could not have completed this work without the unwavering support and belief in me of my family and friends. I would also like to offer special thanks to Bc. Jakub Julius Šmýkal for providing a 3D model of Chandrayaan-3.

# Contents

<b>1</b>	<b>Introduction</b>	<b>8</b>
<b>2</b>	<b>Lunar Lander Mission: Chandrayaan-3</b>	<b>10</b>
2.1	Evolution of Previous Missions in the Chandrayaan Programme . . . . .	10
2.2	Spacecraft: Design, Launch Vehicle and Payload . . . . .	12
2.3	Mission Timeline: From Launch to Descent and Ascent . . . . .	15
2.4	Powered Descent Profile . . . . .	18
<b>3</b>	<b>Descent Trajectory Physics for Lunar Landing</b>	<b>21</b>
3.1	Definitions and Assumptions . . . . .	21
3.2	Coordinate Systems and Reference Frames . . . . .	22
3.3	Newton's Laws of Motion . . . . .	25
3.4	Derivation of the Equations of Motion: The Two-Body Problem . . . . .	26
3.5	Finalised Equations of Motion . . . . .	29
<b>4</b>	<b>Optimal Descent Trajectory</b>	<b>31</b>
4.1	Optimisation Problem Theory . . . . .	31
4.2	Implementation of Optimal Descent Trajectory . . . . .	35
4.3	Results . . . . .	42
<b>5</b>	<b>Design and Implementation of Visualisation Environment</b>	<b>45</b>
5.1	Application Design . . . . .	45
5.2	Application Implementation . . . . .	46
<b>6</b>	<b>Results and Potential Improvements</b>	<b>50</b>
<b>7</b>	<b>Conclusion</b>	<b>52</b>
<b>Bibliography</b>		<b>53</b>
<b>A</b>	<b>Astronomical Bodies and Launch Vehicle in Chandrayaan-3 Mission</b>	<b>57</b>
<b>B</b>	<b>Additional Specifications</b>	<b>59</b>
<b>C</b>	<b>Contents of Associated Media Drive</b>	<b>60</b>

# List of Figures

2.1	Comparison of Chandrayaan-1, Chandrayaan-2 and Chandrayaan-3. . . . .	11
2.2	Chandrayaan-3—Integrated Module encapsulated within LVM3’s payload fairing. Source: [17]. . . . .	12
2.3	Chandrayaan-3—Propulsion Module. Source: [17]. . . . .	13
2.4	Chandrayaan-3—LL and Rover. Source: [17]. . . . .	14
2.5	Launch and TLI of Chandrayaan-3. . . . .	15
2.6	LOI of Chandrayaan-3. . . . .	16
2.7	Landing sites for Chandrayaan-3. Source: [7]. . . . .	17
2.8	Chandrayaan-3 on its way back to Earth. Source: [26]. . . . .	18
2.9	Chandrayaan-3 Lander Powered Descent. Source: [55]. . . . .	19
3.1	Coordinate systems. . . . .	23
3.2	Two-dimensional inertial, body and rotating polar frames of reference. . . . .	23
3.3	LL’s roll, pitch and yaw. . . . .	24
3.4	3D model of Chandrayaan-3 Lander. . . . .	24
3.5	Two-body system in an inertial frame of reference. . . . .	26
3.6	Non-rotating and orbit frames. . . . .	27
3.7	The LL in the frame of reference. . . . .	28
3.8	Radial and tangential velocity. . . . .	29
4.1	One-dimensional convexity. . . . .	32
4.2	Midpoint method. Source: [8]. . . . .	34
4.3	Main window of the Bocop GUI. . . . .	36
4.4	The optimal descent trajectory profile over time (Part 1). . . . .	43
4.5	The optimal descent trajectory profile over time (Part 2). . . . .	44
5.1	Application Frontend. . . . .	46
5.2	Application Design in Godot. . . . .	47
5.3	Bézier curve with knots and control points. . . . .	49
A.1	The Earth. Source: [46]. . . . .	57
A.2	The Moon. Source: [43]. . . . .	57
A.3	LVM3-M4 rocket. Source: [20]. . . . .	58

# List of Tables

4.1	Constant values used in the optimal descent trajectory. . . . .	38
4.2	State variable bounds of the problem. . . . .	39
4.3	Initial and final conditions for Rough Braking Phase . . . . .	40
4.4	Initial and final conditions for Attitude Hold Phase . . . . .	40
4.5	Initial and final conditions for Fine Braking Phase . . . . .	41
4.6	Initial and final conditions for Terminal Descent Phase . . . . .	41
4.7	Segmentation of the Computed Optimal Descent Trajectory . . . . .	42
A.1	Earth specifications. Source: [9, 40]. . . . .	57
A.2	Moon specifications. Source: [9, 40]. . . . .	57
A.3	LVM3-M4 specifications. Source: [20, 50]. . . . .	58
B.1	S200 technical specifications. Source: [20, 21, 50]. . . . .	59
B.2	Vikas engine technical specifications. Source: [3, 20, 50]. . . . .	59
B.3	CE-20 technical specifications. Source: [3, 20, 50]. . . . .	59

# List of Abbreviations

Abbreviation	Meaning
Al	Aluminium
AM	Ante Meridiem (Before Midday)
APXS	Alpha Particle X-Ray Spectrometer
C25	Cryogenic Upper Stage
Ca	Calcium
CE-20	Cryogenic Rocket Engine
ChaSTE	Chandra's Surface Thermophysical Experiment
COVID-19	Coronavirus Disease 2019
DEO	Deorbit Manoeuvre / Burn
EBN	Earth-Bound Manoeuvre
EOM	Equation of Motion
Fe	Iron
GTO	Geosynchronous Transfer Orbit
HTPB	Hydroxyl-Terminated Polybutadiene
ILSA	Instrument for Lunar Seismic Activity
IRAP	Inertial Reference unit and Accelerometer Package
ISRO	Indian Space Research Organisation
IST	Indian Standard Time
ISTRAC	ISRO Telemetry, Tracking and Command Network
K	Potassium
L110	Liquid Core Booster
LBN	Lunar-Bound Manoeuvre
LH <sub>2</sub>	Liquid Hydrogen
LIBS	Laser Induced Breakdown Spectroscope
LL	Lunar Lander
LOI	Lunar Orbit Insertion
LOX	Liquid Oxygen
LRA	Laser Retroreflector Array
LVM3	Geosynchronous Satellite Launch Vehicle Mark III
Mg	Magnesium
MMH	Monomethylhydrazine
MON3	Methylhydrazine with 3% Nitric Oxide
N <sub>2</sub> O <sub>4</sub>	Dinitrogen Tetroxide
NASA	National Aeronautics and Space Administration
NLP	Nonlinear Programming

OCP	Optimal Control Problem
PM	Propulsion Module
PM	Post Meridiem (After Midday)
RAMBHA	Radio Anatomy of Moon Bound Hypersensitive ionosphere and Atmosphere
S200	Solid Strap-on Motor
SDSC	Satish Dhawan Space Centre
SHAPE	Spectro-polarimetry of HABitable Planet Earth
Si	Silicon
SOI	Sphere of Influence
SRB	Space Shuttle Solid Rocket Boosters
TEI	Trans-Earth Injection
Ti	Titanium
TLI	Trans-lunar Injection
UDMH	Unsymmetrical Dimethylhydrazine
UH <sub>25</sub>	Fuel Mixture for Rockets
UTC	Coordinated Universal Time

# Nomenclature

## Greek characters

$\alpha$	Angular acceleration
$\theta$	Angular coordinate in polar coordinate system
$\mu$	Moon's gravitational parameter
$\psi$	Pitch angle
$\omega$	Angular velocity

## Lowercase letters

$\vec{a}$	Acceleration vector
$a_0$	Centrifugal acceleration
$a_\theta$	Acceleration tangential component
$a_r$	Acceleration radial component
$\vec{a}_T$	Engine acceleration
$\hat{b}_x$	Unit vector $x$ component in body Cartesian reference frame
$\hat{b}_y$	Unit vector $y$ component in body Cartesian reference frame
$f$	Objective function
$\hat{i}_\theta, \hat{j}$	Unit vector $\theta$ component in rotating polar reference frame
$\hat{i}_r, \hat{i}$	Unit vector $r$ component in rotating polar reference frame
$\hat{i}_x, \hat{m}$	Unit vector $x$ component in inertial Cartesian reference frame
$\hat{i}_y, \hat{n}$	Unit vector $y$ component in inertial Cartesian reference frame
$k_E$	Engine throttle command
$m$	Mass
$\vec{p}$	Momentum
$r$	Radial coordinate in polar coordinate system

$\vec{r}$	Relative position
$\dot{r}$	Velocity
$\ddot{r}$	Acceleration
$t$	Time
$\vec{v}$	Velocity vector
$v_\theta$	Velocity tangential component
$v_r$	Velocity radial component

### Uppercase letters

<b>B</b>	Bézier curve
$\vec{F}$	Resultant of forces
$G$	Universal gravitational constant
$G_M$	Moon's centre of gravity
$H$	Hessian matrix
$I_{sp}$	Engine specific impulse
$\mathcal{J}$	Cost function
<b>K</b>	Knot point
<b>P</b>	Control point
$\vec{R}_1$	Mass $m_1$ position
$\vec{R}_2$	Mass $m_2$ position
$R_{eq}$	Moon's equatorial radius
$T_{\max}$	Engine maximum thrust
$V_{ex}$	Engine exhaust velocity

# Chapter 1

## Introduction

Exploring space has been one of humanity's greatest endeavours, marked by daring ventures into the unknown and an incessant search for answers. Leading the way in this grand journey is the monumental achievement of lunar landing, showing human ingenuity and enthusiasm for exploration. Looking back on the immense milestones of the past, we can also gaze at the horizon of thrilling projects that the National Aeronautics and Space Administration (NASA) and other space agencies are planning. These undertakings will reshape our connection with the universe.

The impact of the Apollo missions resonates strongly within our collective memory, guiding and inspiring many generations of explorers. Yet, as we shift our view to the future, the Moon once again emerges as a central focus of human ambition. NASA's Artemis program, drawing its name from the twin sister of Apollo and goddess of the Moon in Greek mythology, ushers in an exciting new era in lunar exploration [44]. With the intention to return humans to the lunar surface by mid-2020s, Artemis envisions sustainable exploration of the Moon, laying the foundation for subsequent missions to Mars and beyond [45]. Although NASA has been a leading competitor in lunar exploration for a significant period, it is important to acknowledge that it is not the sole contender in this cosmic pursuit. An increasing number of space agencies worldwide, such as the Indian Space Research Organisation (ISRO), are now stepping up to participate in missions aimed at investigating the Moon.

The significance of an optimal descent trajectory in lunar landing is in its direct influence on the success and safety of lunar missions. By identifying the most efficient and precise path for a spacecraft to descend and land on the surface of the Moon, researchers can minimise fuel consumption, reduce landing uncertainties and enhance the overall mission performance. Additionally, an optimal descent trajectory contributes to the longevity of lunar exploration missions by maximising the payload capacity and enabling targeted landing site selection.

This work is determined to build a theoretical base for the computation of an optimal lunar descent trajectory for the Chandrayaan-3 mission. Moreover, it comes with an application that visualises the final calculated trajectory in a 3D environment. Finally and above all, an assessment of the achieved results can be found at the end of this thesis.

In [Lunar Lander Mission: Chandrayaan-3](#), one has the option to read about the history of all Chandrayaan missions. In addition, the spacecraft's specifications and launch details are provided. [Descent Trajectory Physics for Lunar Landing](#) introduces the lunar landing problem and is dedicated to the descent trajectory physics, along with the equations of motion (EOM) essential for forthcoming computations. In [Optimal Descent Trajec-](#)

**tory**, the collected information and knowledge are utilised for the computation of the optimal descent trajectory of the Lunar Lander (LL). The calculations were made using Bocop, an optimal control problem (OCP) solver and results are presented in the form of graphs. Moving forward, **Design and Implementation of Visualisation Environment** describes the implementation details of the application for visualising computed trajectories, created with the assistance of the 3D engine Godot. **Results and Potential Improvements** discusses the evaluation of the accomplished results, comparing them with the actual trajectories of the Chandrayaan-3 mission and proposing potential improvements for the future. In **Conclusion**, one can find a summary of the thesis. Appendix **A** contains the specifications of the Earth, Moon and launch vehicle—the LVM3-M4 rocket. Appendix **B** offers additional technical specifications that could not be accommodated within the main text. Lastly, Appendix **C** lists the contents of the associated media drive.

## Chapter 2

# Lunar Lander Mission: Chandrayaan-3

This chapter addresses the brief history of the Chandrayaan programme. Afterwards, basic information about the vehicles and spacecraft is provided. Ultimately, a detailed description of the flight is introduced.

### 2.1 Evolution of Previous Missions in the Chandrayaan Programme

The “Chandrayaan programme” constitutes a series of active lunar missions led by ISRO, intended for the exploration of the Moon [16].

The program commenced in 2008 with the launch of Chandrayaan-1, India’s first pioneering venture into deep space exploration. On 12 November 2008, the spacecraft underwent several manoeuvres to attain its operational polar orbit at a height of 100 km above the lunar surface to map the exterior of the Moon and analyse its mineral composition. In late November 2008, Chandrayaan-1 faced atypically high temperatures, limiting its operation to solely one scientific instrument at a time out of its total of 11. It appears that in an effort to regulate the temperatures, the spacecraft’s orbit was raised to 200 km in May 2009. The mission was terminated on 29 August 2009 [16], following the loss of contact with Chandrayaan-1. Although the spacecraft’s projected two-year operational lifespan was abruptly shortened, mission objectives were finished by at least 95 %, as reported by ISRO. The presumed cause of the mission’s premature end was an overheating-related power supply failure [36].

Chandrayaan-2 is ISRO’s second lunar exploration mission, marking an exceptional technological advancement compared to its predecessors. It consisted of an orbiter and an LL carrying a Rover, all of which were developed in India. The mission’s main objective was to showcase the capability of soft-landing on the Moon and navigating a robotic Rover on the surface [37]. From scientific perspective, the goals included [19]:

- studying lunar topography, mineralogy, elemental abundance, the lunar exosphere, and detecting signatures of hydroxyl and water ice,
- investigating the presence of water ice in the south polar region and the thickness of the lunar regolith on the surface,
- mapping the lunar surface and contributing to the preparation of 3D maps of it.

Chandrayaan-2 was launched on 22 July 2019 from Satish Dhawan Space Centre (SDSC) on Sriharikota Island, employing the ISRO's Geosynchronous Satellite Launch Vehicle Mark III (LVM3). After a sequence of Earth-bound (EBN) and lunar-bound manoeuvres (LBN), the spacecraft entered a circular polar orbit around the Moon. Once the Lander separated from the orbiter, deorbit manoeuvres (DEO) and powered descent took place. Everything proceeded as expected until the Lander was just 2.1 km above the surface when it started diverging from its originally planned trajectory. At that moment, communication with the Lander and ground station was lost, resulting in the LL crashing on the surface. It apparently remained intact, but all further operations were unachievable. Despite the fact that the Rover was not deployed, the Chandrayaan-2's orbiter continues to operate around the Moon [15].

After the setback of Chandrayaan-2, two months elapsed before a proposal for a third deep space mission emerged, focusing on the Lander and Rover as the most important elements of the spacecraft. ISRO sought to learn from previous mistakes and prevent their recurrence by implementing extra modifications to the LL. An overview of all Chandrayaan models and their basic distinctions can be noticed in Figure 2.1. The launch, originally scheduled for early 2021, was held up until 2022 due to the COVID-19 pandemic in India. Additional tests and a few more adjustments needed to be conducted thereafter, thus postponing the launch date to the second quarter of 2023 [13].

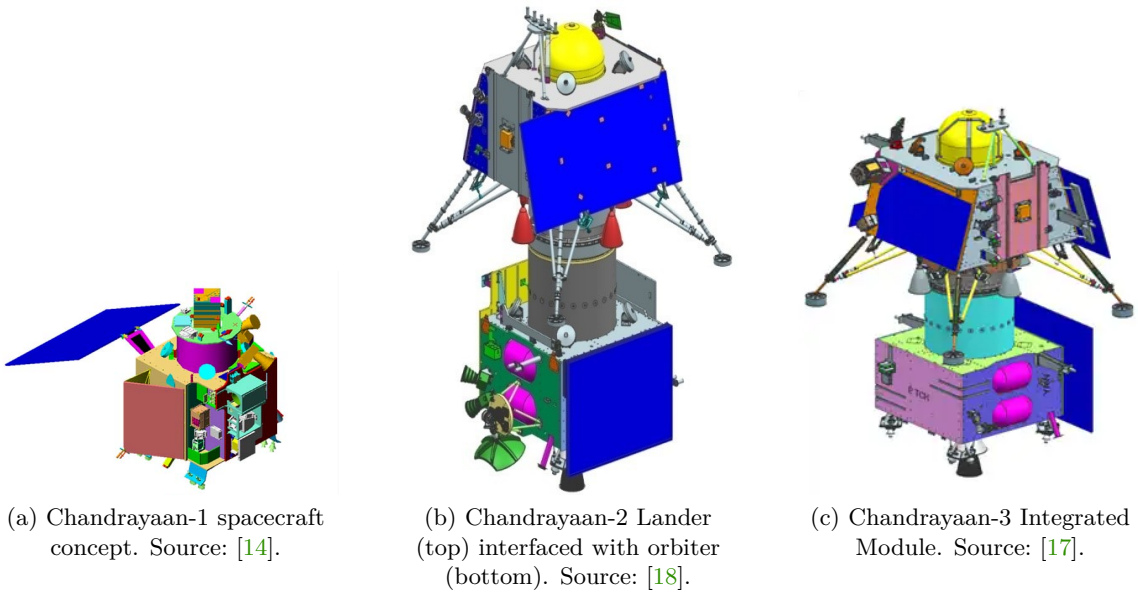


Figure 2.1: Comparison of Chandrayaan-1, Chandrayaan-2 and Chandrayaan-3.

With the inception of a new mission, new objectives arose. The main purpose of setting Chandrayaan-3 in motion was to demonstrate a risk-free soft landing on the Moon's exterior. If the first objective is completed without encountering any hazardous outcomes, two further objectives could potentially be feasible. The primary goal among these is to show how the Rover roams on the lunar surface, while the other involves performing in-situ scientific experiments. To accomplish all the mission objectives, the Lander is equipped with several advanced technologies, which will be discussed in the next section [17].

## 2.2 Spacecraft: Design, Launch Vehicle and Payload

The Chandrayaan-3 spacecraft was launched atop the LVM3-M4 rocket, as seen in Figure 2.2. LVM3 fulfils ISRO’s role as a heavy lift launch vehicle, boasting an impressive record of completing six sequential successful missions. The aim of LVM3’s current fourth operational flight was to place the Chandrayaan-3 spacecraft into Geosynchronous Transfer Orbit (GTO) [17].

Chandrayaan-3 comprises a LL and Rover nearly identical to those used in the Chandrayaan-2 mission, along with a Propulsion Module (PM) responsible for conveying the spacecraft from Earth orbit to lunar orbit.



Figure 2.2: Chandrayaan-3—Integrated Module encapsulated within LVM3’s payload fairing. Source: [17].

### LVM3-M4 Rocket

LVM3 is constructed as a three-stage rocket, incorporating two solid strap-on motors (S200), one liquid core stage (L110) and a high-thrust cryogenic upper stage (C25). The S200 is one of the world’s largest solid boosters, containing over 205 t of solid propellant [28]. The L110 utilises a twin-engine configuration and carries approximately 115 t of liquid propellant. Concurrently, the C25 features the fully indigenous high-thrust cryogenic engine (CE-20) and holds about 28 t of propellant. The entire length of the vehicle is 43.5 m, featuring a payload fairing with a diameter of 5 m. The payload capacity includes 8 000 kg to Low Earth Orbit (LEO), 4 000 kg to GTO and 3 000 kg to Trans-lunar Injection (TLI) [50].

Two S200s power the first stage, producing a combined thrust of 5 150 kN at take-off. The solid-fuel booster ranks among the hugest after the Space Shuttle Solid Rocket Boosters

(SRB) and its flex nozzles play a crucial role in steering the vehicle during the initial ascent phase. The second stage is driven by a pair of Vikas engines, each generating 805.5 kN of thrust. Compared to prior Indian rockets, the Vikas engines are now equipped with a regenerative cooling, which enhances both weight efficiency and specific impulse. The final stage is propelled by a single CE-20, delivering about 200 kN of thrust. From the LVM3-M3 mission onward, a newly introduced white C25 incorporates significantly more environmentally friendly manufacturing processes, improved insulation properties and lightweight materials [20]. Appendix A contains additional technical specifications of the rocket. Further details about each rocket engine can be found in Appendix B.

## Propulsion Module

The PM features a box-like design based on the modified I-3K structure. It encompasses a large solar panel attached to one side and a cylinder on top, known as the Intermodule Adapter Cone, which serves as the mounting structure for the LL. The main thruster nozzle is located at the bottom of the PM. The module weighs 2 145.01 kg, including 1 696.39 kg allocated to the monomethylhydrazine (MMH) and dinitrogen tetroxide (MON3) bipropellant propulsion system. It can produce 738 W of power and communicates through S-band. The attitude sensors consist of a star sensor, a sun sensor and an Inertial Reference unit and Accelerometer Package (IRAP). In Figure 2.3, one can see all elementary parts of the PM [38]. The primary function of the PM was to transport the Lander from launch vehicle injection orbit to the final 100 km circular polar orbit around the Moon and then to separate the LL from the PM. On top of that, it carried the Spectro-polarimetry of HAbitable Planet Earth (SHAPE) payload to examine the spectral and polarimetric measurements of Earth from the lunar orbit [17].

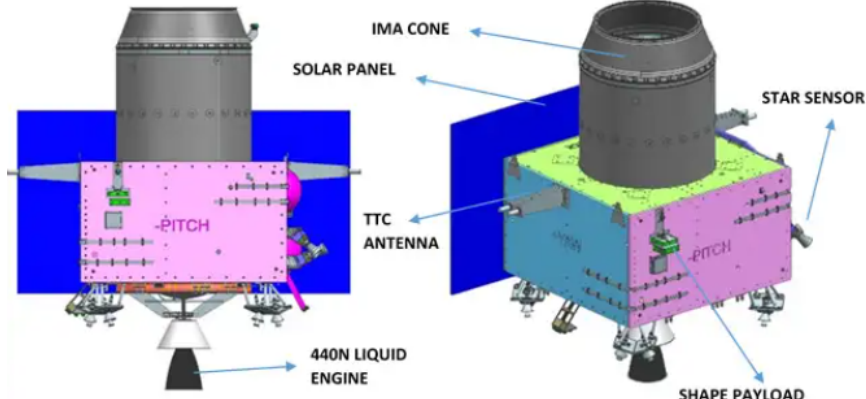


Figure 2.3: Chandrayaan-3—Propulsion Module. Source: [17].

## Vikram Lander

Named after Indian space program pioneer Vikram Sarabhai, the Vikram Lander has a box-like shape measuring  $200 \times 200 \times 116.6$  cm. It is equipped with four landing legs and four landing thrusters. The lander weighs precisely 1 749.86 kg (dry mass of Vikram and 1 042.38 kg of propellant mass [49]), which includes 26 kg allocated for the Rover. It is capable of generating 738 W using solar panels mounted on its sides. The LL features various sensors to guarantee a secure touchdown, such as an accelerometer, altimeters

(Ka-band and laser), Doppler velocimeter, star sensors, inclinometer, touchdown sensor and a collection of cameras for hazard avoidance and positional awareness. An attitude control is managed by reaction wheels, while propulsion is facilitated through an MMH and MON3 bipropellant system comprising four 800 N throttle-able engines and eight 58 N throttle-able engines. Communication is handled by an X-bang antenna [38]. Figure 2.4 (a) shows the Vikram with a detailed description of all components. The Lander is designed to perform a soft landing at a specified lunar site and deploy the Rover onto the surface using a ramp.

The Vikram Lander was equipped with several instruments: the Radio Anatomy of Moon Bound Hypersensitive ionosphere and Atmosphere (RAMBHA) to measure near-surface plasma density and track its changes over time, the Chandra's Surface Thermophysical Experiment (ChaSTE) for assessing the thermal conductivity and temperature of the lunar exterior near polar region, the Instrument for Lunar Seismic Activity (ILSA) for monitoring seismicity around the landing site and mapping the structure of the lunar crust and mantle and a passive Laser Retroreflector Array (LRA) from NASA, used as a reference point on the lunar surface [17, 33].

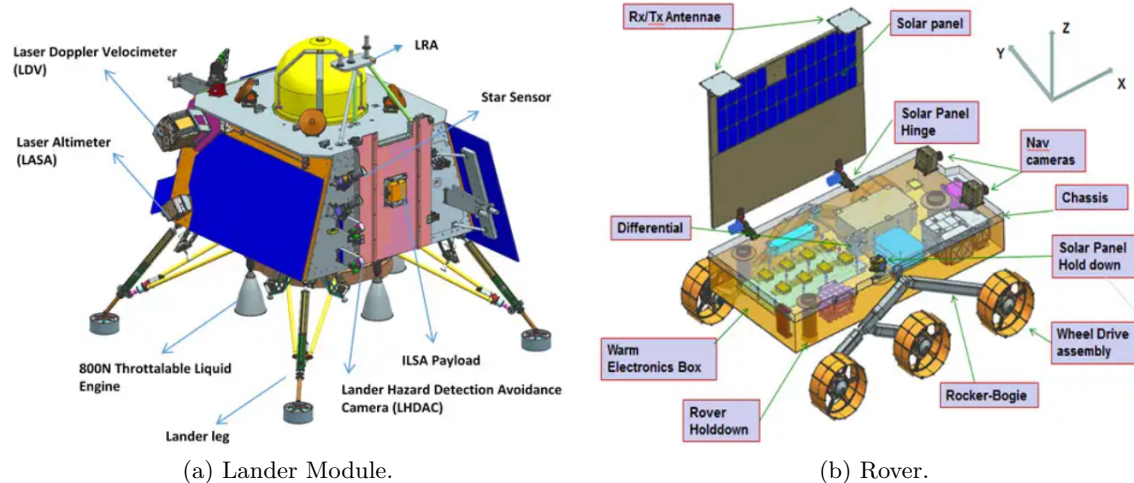


Figure 2.4: Chandrayaan-3—LL and Rover. Source: [17].

## Pragyan Rover

The Pragyan Rover (Sanskrit for “wisdom”) features a rectangular chassis measuring  $91.7 \times 75.0 \times 39.7$  cm, installed on six-wheel rocker-bogie wheel drive assembly. It possess navigation cameras and a solar panel generating 50 W of power. Communication with the LL is achieved by Rx/Tx antennas [38]. In Figure 2.4 (b), one can see a portrayal of the Rover.

The Pragyan Rover utilises two instruments: an Alpha Particle X-Ray Spectrometer (APXS) to analyse the chemical composition and infer mineralogical details, enhancing our understanding of the lunar surface and a Laser Induced Breakdown Spectroscopy (LIBS) to ascertain the elemental composition (Magnesium (Mg), Aluminium (Al), Silicon (Si), Potassium (K), Calcium (Ca), Titanium (Ti), Iron (Fe)) of lunar soil and rocks in the vicinity of the Moon’s touchdown [17].

## 2.3 Mission Timeline: From Launch to Descent and Ascent

### Launch

The initial phase of the mission involved pre-launch procedures, liftoff and ascent of the launcher and a sequence of EBNs conducted while the spacecraft was still in Earth's vicinity. Chandrayaan-3 was launched on 14 July 2023 at 09:05 AM UTC (02:35 PM IST) from SDSC in Shiharikota, India, using ISRO's LVM3. Just over 15 minutes later, at 09:21 AM UTC, Chandrayaan-3 was placed into an Earth parking orbit with a perigee of 170 km and an apogee of 36 500 km after separation from LVM3. On 15 July 2023, the first orbit-raising manoeuvre was carried out by ISRO Telemetry, Tracking and Command Network (ISTRAC), leaving the spacecraft in a highly elliptical  $173 \text{ km} \times 41\,762 \text{ km}$  orbit. Following this, four supplementary Earth-bound perigee firings were executed [22]. Figure 2.5 (a) shows the location of Chandrayaan-3 after the fifth EBN.

### Trans-lunar Injection

In the second phase of Chandrayaan-3, the spacecraft departed from Earth's orbit and then performed the TLI in order to get to the Moon. A series of EBNs gradually increased Chandrayaan-3's speed for the TLI. The spacecraft was propelled by this acceleration into a Trans-lunar orbit, where its apogee was expanded sufficiently to be captured by the Moon's gravity and enter lunar orbit. On 1 August, the TLI was completed, positioning Chandrayaan-3 into a  $288 \text{ km} \times 369\,328 \text{ km}$  lunar orbit [23]. It took a total of four days for the spacecraft to reach the Moon. In Figure 2.5 (b), one can witness Chandrayaan-3 at end of its lunar transfer trajectory.

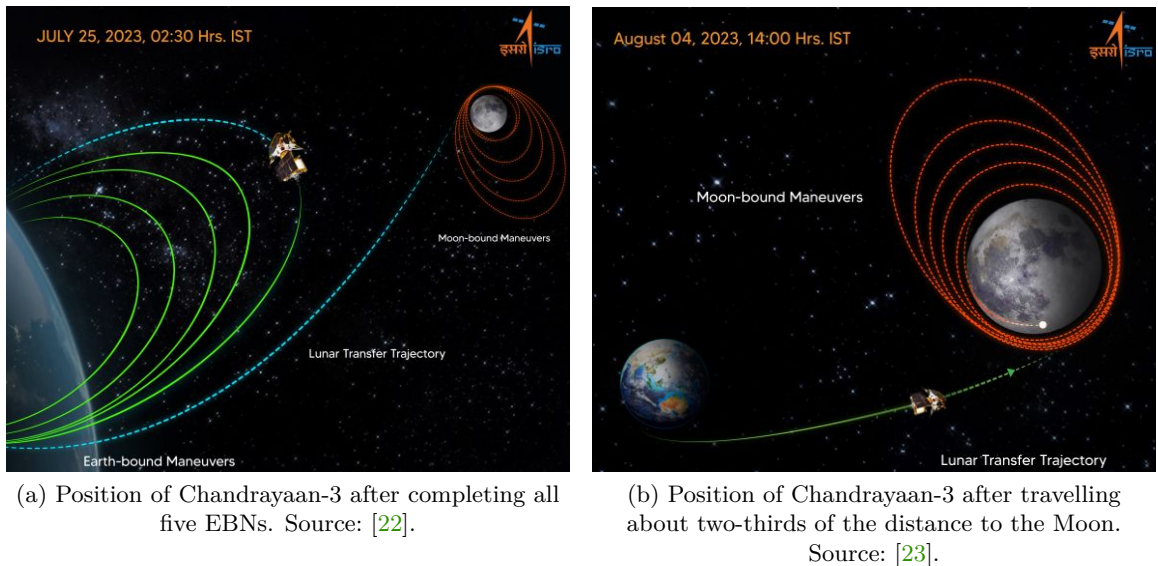


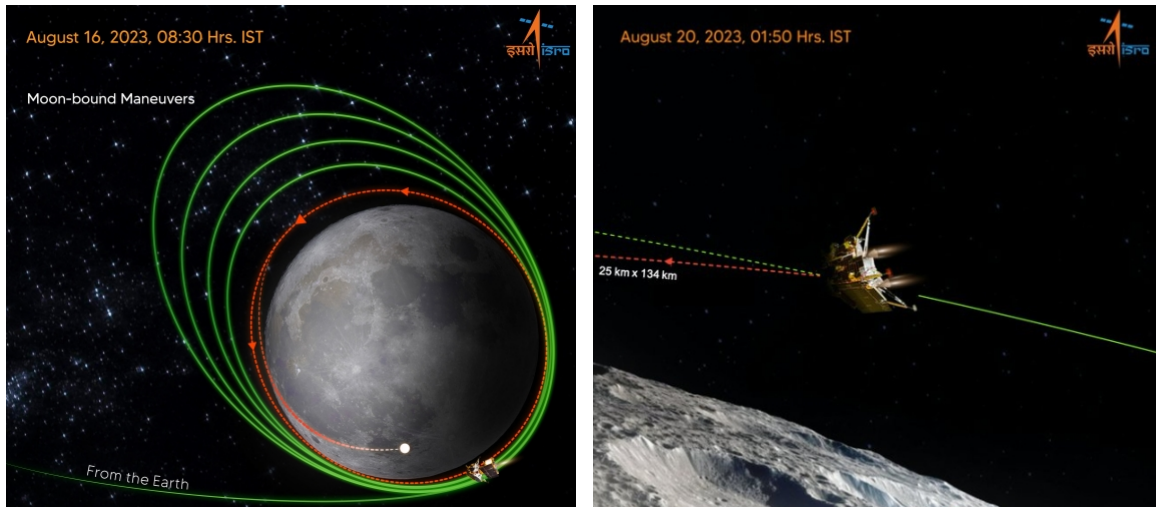
Figure 2.5: Launch and TLI of Chandrayaan-3.

### Lunar Orbit Insertion

In the third phase of Chandrayaan-3, the mission began with Lunar Orbit Insertion (LOI). Multiple LBNs were crucial for reducing the eccentricity of the lunar orbit, achieved through

several retrograde burns conducted at perilune. Subsequently, the PM and LL separated, followed by deboosting and a pre-landing phase for the LL prior to its touchdown on the lunar surface. Upon landing, the LL and Rover commenced their operational phase, which lasted one lunar day and was dedicated to surface experiments.

On 5 August, Chandrayaan-3 entered a lunar orbit measuring  $164 \text{ km} \times 18\,074 \text{ km}$  following a 30-minute engine firing. Afterwards, the PM carried out a series of burns to shorten a Chandrayaan-3's orbit, positioning it closer to the Moon's surface in preparation to set apart from the LL. Extra firings by the PM put the spacecraft into a polar lunar orbit with an altitude of  $153 \text{ km} \times 163 \text{ km}$  by 17 August. Chandrayaan-3's position on this date is shown in Figure 2.6 (a). On 17 August, the LL separated from the PM. The first deboosting was completed on 18 August, placing the LL in a  $113 \text{ km} \times 157 \text{ km}$  orbit. The second and final manoeuvre, DEO, was finished on 20 August, adjusting the LL's orbit to  $25 \text{ km} \times 134 \text{ km}$  [7]. Figure 2.6 (b) displays the spacecraft before its powered descent.



(a) Position of Chandrayaan-3 after finalising all five LBNs. Source: [24]. (b) Position of Chandrayaan-3 after second DEO. Source: [25].

Figure 2.6: LOI of Chandrayaan-3.

## Landing

On 23 August, as the LL approached the lowest point of its orbit, its four engines completed a braking manoeuvre at  $30 \text{ km}$  above the lunar surface. After 11.5 min (690 s), the spacecraft descended to an altitude of  $7.2 \text{ km}$ . It maintained this height above the ground for about 10 s before initiating another braking phase. Using two engines, it slowed its descent to roughly  $150 \text{ m}$ , then hovered for about 30 s to select an optimal landing spot. The LL persisted in a vertical orientation as it touched down at 12:33 AM UTC (06:03 PM IST), positioned at  $69.367\,621^\circ \text{ S}, 32.348\,126^\circ \text{ E}$ .

The landing site for Chandrayaan-3 was chosen from eight contemplated locations, with two final options designated as primary and alternate (backup) sites. The touchdown spot is circa  $42 \text{ km}$  from Chandrayaan-2's scheduled landing site, situated between Manzius U and Boguslawsky craters. This decision was meticulously made, considering

various factors such as safe landing and roving, illumination, temperature, geological composition and environmental characteristics conducive to scientific exploration [7]. The area mentioned above can be recognised in Figure 2.7.

On 24 August, the Pragyan Rover descended from Vikram's ramp to the lunar surface, where it conducted experiments. Both the Lander and Rover were designed to operate throughout one lunar day, equivalent to approximately 14 Earth days.

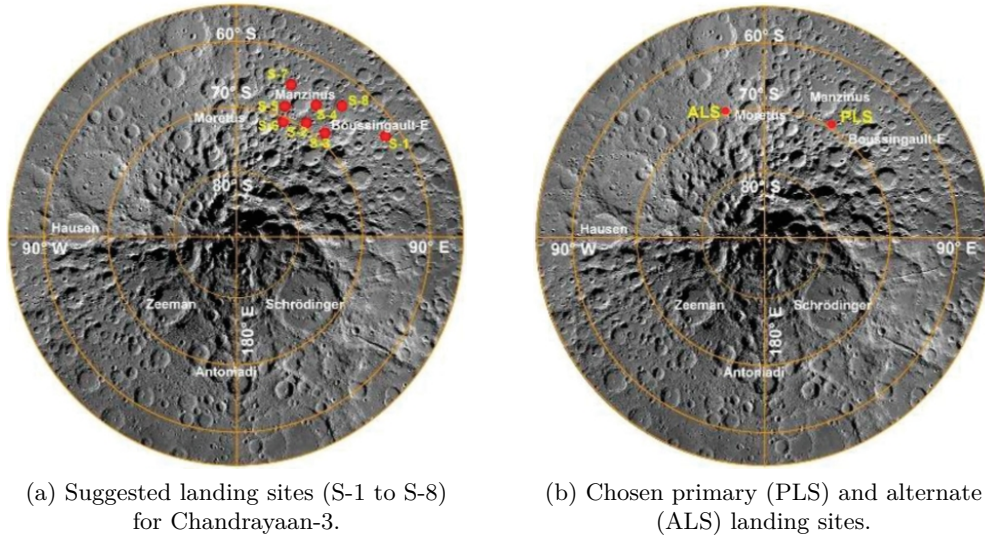


Figure 2.7: Landing sites for Chandrayaan-3. Source: [7].

## Ascent and Trans-Earth Injection

Vikram performed a “Hop experiment” on 3 September, lifting the module 40 cm off the lunar surface before touching down again. This demonstration showcased the module’s capability to ascend from the Moon, a potential asset for future sample return missions. The experiment was regarded as a “bonus objective” of the mission plan and was executed by the LL’s onboard computer. On 4 September, both the Lander and Rover entered sleep mode and subsequent attempts to establish communication on 22 September were unsuccessful [7].

On 4 December, the PM shifted from a lunar orbit to an Earth. The PM’s main task was to carry the LL from GTO to the circular lunar polar orbit and then detach from the LL. A preliminary plan was to manipulate the SHAPE payload for about three months. Thanks to the accurate orbital injection by LVM3 and the effective manoeuvres, the PM concluded its initial month of operations with over 100 kg of fuel remaining. This excess fuel allowed for the collection of additional data for future lunar missions and demonstrated operational strategies for a potential sample return mission [7].

On 9 October 2023, the first manoeuvre elevated the apogee from 150 km to 5 112 km, thereby extending the orbital period from 2.1 hours to 7.2 hours. In Figure 2.8 (a), one can see the location of Chandrayaan-3 prior to (green) and after (magenta) the manoeuvre. Following a reassessment of available propellant, the plan for the second manoeuvre was revised to target an Earth orbit spanning 180 000 km by 380 000 km. On 13 October, the Trans-Earth Injection (TEI) was carried out. Subsequently, the PM completed four

additional Moon flybys before exiting the lunar sphere of influence (SOI) on 10 November, with its first perigee crossing occurring on 22 November at an altitude of 154 000 km. Currently, the PM orbits Earth with its perigee and apogee altitudes changing throughout its trajectory. The predicted lowest perigee altitude is 115 000 km and the orbital period is approximately 13 days with a 27° inclination. Figure 2.8 illustrates the PM’s trajectory towards Earth (b). The SHAPE payload works whenever Earth is within its field of view, including during extraordinary events like lunar eclipses. Operations involving the SHAPE payload are intended to continue as planned [26].

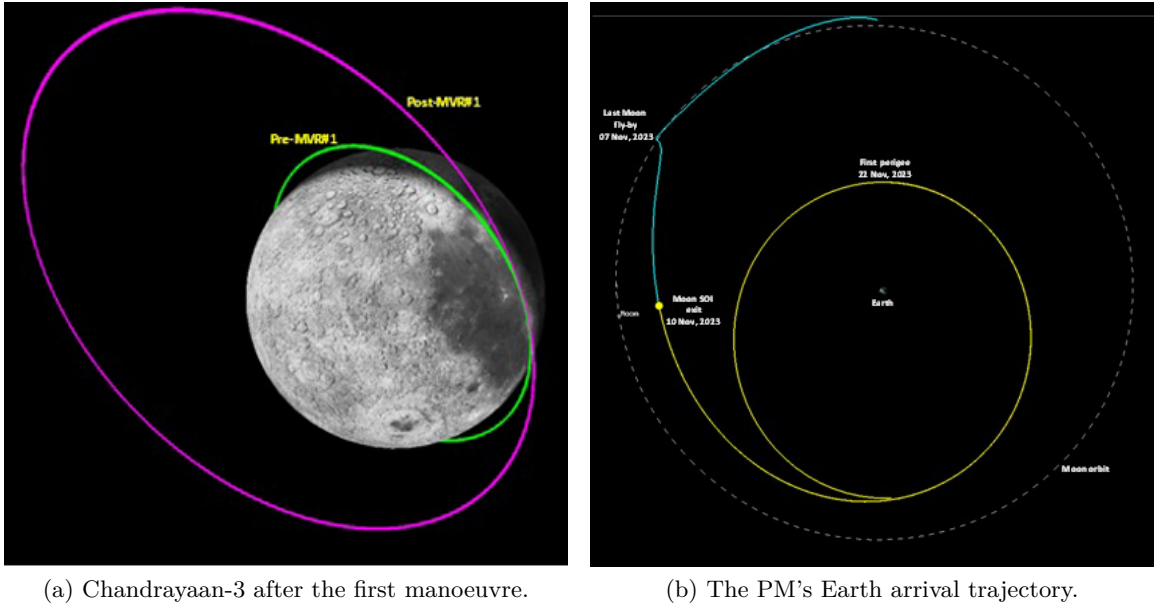


Figure 2.8: Chandrayaan-3 on its way back to Earth. Source: [26].

## 2.4 Powered Descent Profile

As outlined above, on 20 August 2023, ISRO’s Chandrayaan-3 mission successfully completed its second DEO. This operation reduced its speed, placing it in a 25 km × 134 km lunar orbit, which was essential for its upcoming soft landing attempt [31]. The most crucial technical manoeuvre occurred on 23 August, during the final 20 min of descent, when the lander had to transition from a high-speed horizontal position to a vertical one, ensuring a gentle descent onto the Moon’s surface. The ensuing discussion draws significant inspiration from an article provided in [27].

The mission’s success hinged on those last 20 min. After ISRO’s decision to terminate the initial Chandrayaan-2 launch attempt in July 2019, K. Sivan, then chairman of India’s space agency, characterised this critical phase as “20 minutes of terror”. Dr. Sivan’s depiction underscored the intricacies of the mission’s final stage, in which Chandrayaan-2 experienced a setback due to the Vikram lander’s incorrect transition from horizontal to vertical. This misstep resulted in the lander’s unintended crash on the lunar surface while approaching the Fine Braking Phase at an altitude of just 7.4 km above. Figure 2.9 portrays the entire powered descent. Further detailed explanations of each phase will follow in the text.

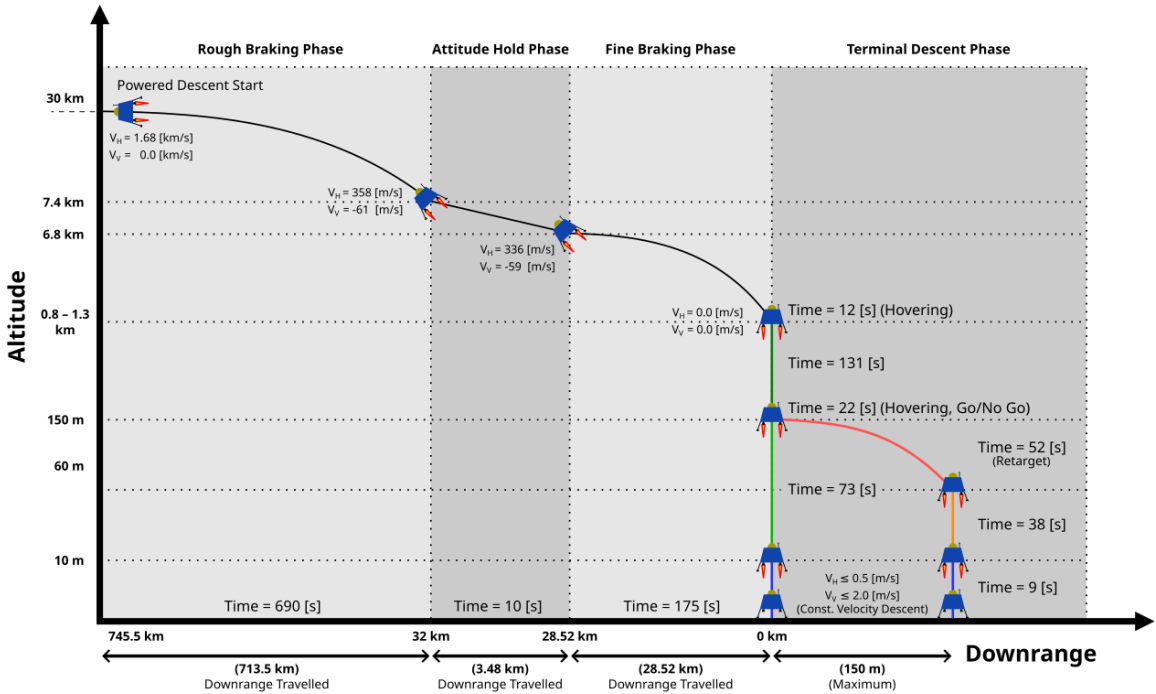


Figure 2.9: Chandrayaan-3 Lander Powered Descent. Source: [55].

The key aspect of Chandrayaan-3’s landing was managing the lander’s speed. The descent began with the spacecraft moving horizontally at  $1\,680 \text{ m} \cdot \text{s}^{-1}$ , with its legs oriented in the direction of travel [31]. Around 06:04 PM IST on 23 August, the spacecraft approached  $70^\circ$  South latitude. Descending from an altitude of 30 km, it had to rotate  $90^\circ$  to align its landing legs with the lunar surface and simultaneously reduce its speed to achieve a near-zero velocity. This manoeuvre also posed a vital challenge during the Chandrayaan-2 mission.

### Rough Braking Phase

The landing sequence started with a horizontal velocity (also known as tangential velocity) of  $1\,680 \text{ m} \cdot \text{s}^{-1}$ , while the vertical velocity (also referred to as radial velocity) remained at zero initially. This speed needed to be reduced to  $358 \text{ m} \cdot \text{s}^{-1}$  horizontally and  $61 \text{ m} \cdot \text{s}^{-1}$  vertically during the optimal *Rough Braking Phase*, lasting 690 seconds. Covering a distance of 713.5 km over the Moon’s surface toward the landing area, the lander descended from an altitude of 30 km to 7.4 km throughout this phase.

### Attitude Hold Phase

Once the spacecraft reached an altitude of 7.4 km, it entered an *Attitude Hold Phase*, maintaining a constant pitch angle for the duration of it. Travelling a distance of 3.48 km, this phase spanned approximately 10 s as the lander transitioned from a horizontal to a vertical position. Subsequently, the height decreased to 6.8 km above the surface, with the tangential velocity reduced to  $336 \text{ m} \cdot \text{s}^{-1}$  and the radial velocity reduced to  $59 \text{ m} \cdot \text{s}^{-1}$ .

## Fine Braking Phase

The *Fine Braking Phase*, marking the third stage of the landing sequence, lasted about 175 s. As it crossed the final 28.52 km to the landing site during this phase, the lander shifted fully into a vertical position. The altitude was brought down to between 800 m and 1 300 m and the lander came to a complete stop with a speed of  $0 \text{ m} \cdot \text{s}^{-1}$ , both horizontally and vertically.

## Terminal Descent Phase

Upon arriving at altitudes of 800 m and 1 300 m, the spacecraft initiated sensor verification to confirm the proper functioning of all onboard systems. The spacecraft, positioned at a height of 150 m above the surface, conducted a hazard assessment to determine whether to proceed with a vertical landing or manoeuvre laterally up to 150 m to evade obstacles such as boulders or craters. The lander was expected to touch down at a maximum radial speed of  $2 \text{ m} \cdot \text{s}^{-1}$  and horizontal speed of  $0.5 \text{ m} \cdot \text{s}^{-1}$  in an ideal scenario.

In this thesis, *Terminal Descent Phase* begins at 1 300 m (where the spacecraft halts during the *Fine Braking Phase*). Furthermore, the option for retargeting up to 150 m will be neglected, with no impediments expected along the way, while all other conditions will be met.

## Chapter 3

# Descent Trajectory Physics for Lunar Landing

First of all, the definitions and assumptions for the lunar landing problem are defined. Coordinate systems are thereafter explained, followed by the establishment of reference frames. The EOM governing the vehicle's movement are formed afterwards. To achieve this, the physics of the problem needs to be discussed. Subsequent sections start with the presentation of Newton's laws of motion, followed by an introduction to the derivation steps and a mention of the EOM.

### 3.1 Definitions and Assumptions

A Moon landing or lunar landing, whether manned or robotic, refers to an event in which people land a spacecraft on the surface of the Moon [34]. Throughout history, this term has been predominantly associated with the Apollo missions carried out by NASA during the 1960s and 1970s. However, the Soviet Union made a remarkable breakthrough in 1966 with the Luna 9 mission, achieving the first successful lunar landing. Luna 9 became the first spacecraft to perform a soft landing on the Moon and relay photographic data back to Earth [39].

The lunar landing problem is a mathematical and engineering hindrance in ensuring the secure touchdown of a spacecraft on the Moon. This challenge involves various factors, such as navigation, propulsion, trajectory planning and landing dynamics, all requiring careful attention to attain a successful and safe landing. Managing descent velocity, steering away from dangerous terrain features and accounting for the Moon's distinctive gravitational conditions are key aspects of this endeavour [42].

As mentioned in master's thesis [12], the Moon finishes one rotation on its own axis in the same amount of time it takes to orbit around the Earth. The speed of the lunar surface at the equator is about  $4.6 \text{ m} \cdot \text{s}^{-1}$ . Imagine aiming for a particular landing spot; in this scenario, the Moon's rotation would become crucial as the site's position would shift relative to the inertial frame. Yet, since there is no specific target, it is logical to ignore the Moon's rotation. To cancel the vehicle's velocity relative to the rotating surface, the additional fuel required would constitute less than 0.3 % of the total fuel consumption. Considering this, it would not discernibly impact the results or trends and can thus be disregarded.

The Moon is presumed to be spherical, lacking an atmosphere. A purely Newtonian gravity model is used, which means it does not account for the gravitational effects

of the Earth and the Sun, or for any changes caused by the Moon’s oblateness—a condition where a round object is flattened at its poles. In space flight mechanics problems, it is frequently assumed that the vehicle’s exhaust velocity remains constant, because the engine’s properties typically do not undergo drastic changes within the operational range.

## 3.2 Coordinate Systems and Reference Frames

### Cartesian Coordinate System

Cartesian coordinates (illustrated in Figure 3.1 (a)), commonly known as rectangular coordinates, are rectilinear coordinates in two or three dimensions. In 2D Cartesian coordinates, the two axes (usually labelled the  $x$ - and  $y$ -axes) are linear and perpendicular to each other. The  $x$ -axis is referred to as the “left and right” or horizontal axis, whereas the  $y$ -axis is viewed as the “up and down” or vertical axis. The coordinates  $x$  and  $y$  can range over the interval  $(-\infty, \infty)$ . An ordered pair  $(x, y)$  is often termed a vector [51].

The system is centred at the origin  $(0, 0)$  and is characterised by two unit vectors,  $\vec{i}$  and  $\vec{j}$ , which are vectors of length one pointing along the positive  $x$ -axis and positive  $y$ -axis, respectively. Vector  $\vec{r}$  is described in Equation 3.1.

$$\vec{r} = x\vec{i} + y\vec{j} \quad (3.1)$$

### Polar Coordinate System

In polar coordinates (one can see in Figure 3.1 (b)),  $r$  indicates the distance from the origin (similar to the radius of a circle) and  $\theta$  stands for the angle measured counterclockwise from the positive  $x$ -axis to the point  $P$ . Here,  $r \in [0, \infty)$  and  $\theta \in [0, 2\pi]$ . This contrasts with Cartesian coordinates, where a point is located based on its perpendicular distances from the  $x$  and  $y$  axes. While Cartesian coordinates specify positions by horizontal and vertical distances, polar coordinates pinpoint them by distance and angle. The polar coordinates are expressed in relation to Cartesian coordinates through Equations 3.2 and 3.3. The representation of a point  $P$  as an ordered pair  $(r, \theta)$ , is known as polar notation [52].

$$x = r \cdot \cos \theta \quad (3.2)$$

$$y = r \cdot \sin \theta \quad (3.3)$$

### Frames of Reference

The initial stage in setting up the descent trajectory physics for the LL involves putting the vehicle into a coordinate system, which enables precise determination of its location. This thesis employs three frames of reference:

- Moon Centred Inertial Frame
- Body Fixed Frame
- Moon Centred Moon Fixed Frame

The vehicle’s motion is confined to a single plane of motion, specifically the Moon’s equatorial plane. This means that the vehicle can only move within a specific flat surface or plane, which in this case is aligned with the equator of the Moon. It suggests that the vehicle’s

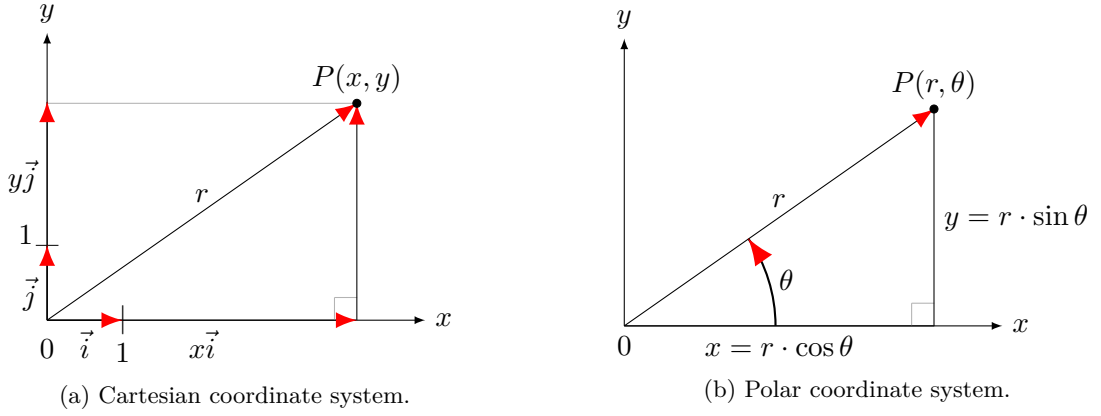


Figure 3.1: Coordinate systems.

movement is limited to two dimensions rather than freely moving in three-dimensional space. In the inertial frame, when we designate the  $x$ - $y$  plane as the motion plane, it consists of the perpendicular unit vectors  $\hat{i}_x$  and  $\hat{i}_y$ . Similarly, in the body frame, the vectors reduce to the two-dimensional perpendicular unit vectors  $\hat{b}_x$  and  $\hat{b}_y$ . A rotating reference frame includes the unit vectors  $\hat{i}_r$  and  $\hat{i}_\theta$ , which rotate synchronously with the vehicle's orbit around the Moon. The vector  $\hat{i}_r$  consistently points from the origin to the vehicle, while  $\hat{i}_\theta$  persists perpendicular to the radius vector and is aligned with the vehicle's direction of motion [12]. Figure 3.2 shows all the reference frames.  $G_M$  indicates the centre of lunar gravity and  $LL$  symbolises the spacecraft (vehicle). Ultimately,  $R_{eq}$  stands for the Moon's equatorial radius. Lines at right angles to each other are portrayed with a perpendicular symbol.

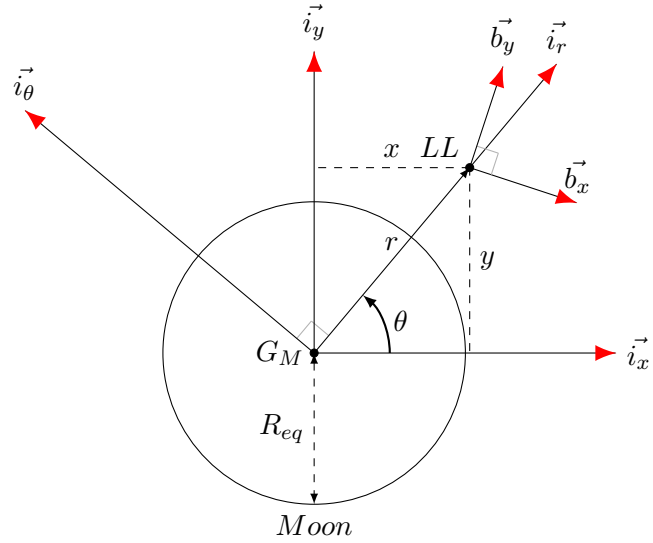


Figure 3.2: Two-dimensional inertial, body and rotating polar frames of reference.

Polar coordinates are selected for computing the optimal descent trajectory due to their mathematical simplifications. To visualise the results in a developed environment, a Cartesian system is used. The LL is simplified to a point mass.

## Chandrayaan-3 Spacecraft Attitude

The spacecraft can rotate unrestrictedly in all three dimensions. Picture three lines running through the vehicle, intersecting at right angles at its centre of gravity. The *roll* angle signifies rotation about the *x*-axis, the *pitch* angle denotes rotation concerning the *y*-axis and the *yaw* angle represents the rotation around the *z*-axis. The rotation axes for Chandrayaan-3 are illustrated in Figure 3.3. A 3D model of the LL, created utilising ISRO's real images of the spacecraft by Bc. Jakub Julius Šmýkal specifically for this thesis, is depicted in Figure 3.4. For the purposes of this thesis, the spacecraft's manoeuvres are restricted to spins around its *y*-axis.

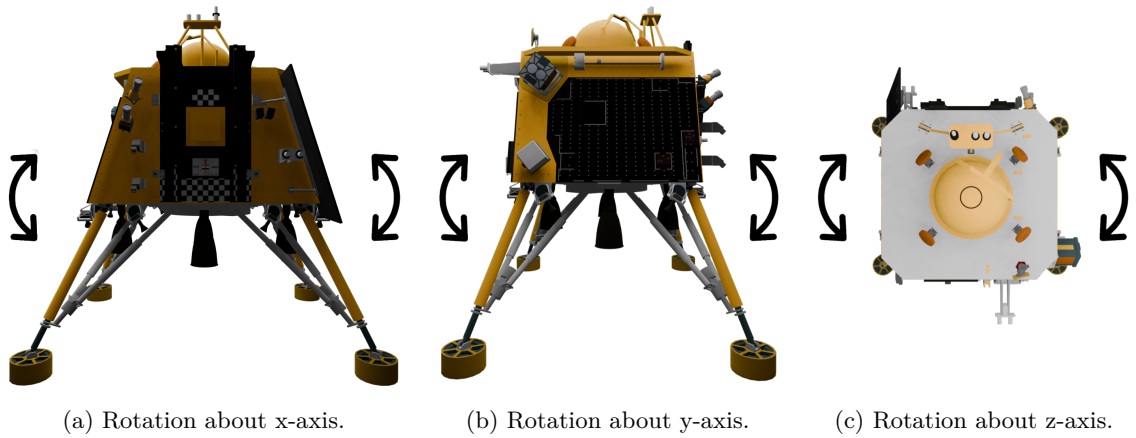


Figure 3.3: LL's roll, pitch and yaw.

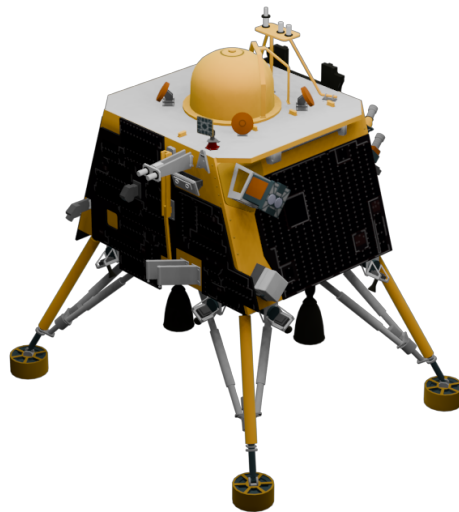


Figure 3.4: 3D model of Chandrayaan-3 Lander.

### 3.3 Newton's Laws of Motion

Newton's three Laws of Motion, along with the Law of Universal Gravitation, play a vital role in deriving the EOMs. The remainder of this section is excerpted from [5].

#### Newton's First Law

"Every object continues in its state of rest or of uniform motion in a straight line unless it is compelled to change that state by forces impressed upon it."

Rephrasing it simpler: Unless acted upon by an external force, objects will either remain at rest or continue moving uniformly in a linear path. This opposition to alterations in motion is called inertia. In a scenario, when all external forces balance each other, the object experiences no net force, leading it to preserve a constant velocity [41]. In other words, the first law necessitates identifying an inertial system where the absolute motion of the object can be defined.

#### Newton's Second Law

"The rate of change of momentum is proportional to the force impressed and is in the same direction as that force."

An easier interpretation: A force is equivalent to the change in momentum (mass multiplied by velocity) divided by the change in time. Momentum is the product of an object's mass  $m$  and its velocity  $v$  [41]. It can be mathematically formulated as in Equation 3.4, where  $\vec{F}$  constitutes the resultant of the forces acting on the object and  $\vec{p} = m\vec{v}$  is regarded as its momentum. In the case of a system with constant mass  $m$ , it is expressed by Equation 3.5, with  $\vec{a}$  standing for the mass's acceleration measured in an inertial reference frame, given by  $\vec{a} = d\vec{v}/dt$ .

$$\vec{F} = \frac{d\vec{p}}{dt} \quad (3.4)$$

$$\vec{F} = m\vec{a} \quad (3.5)$$

An equation differs when considering a variable-mass system, for example, a rocket launcher, where the change of mass per unit time ( $\dot{m}$ ) is notable. In such instances, the EOM is modified accordingly, as shown in Equation 3.6.

$$\vec{F} = m\vec{a} + \dot{m}\vec{v} \quad (3.6)$$

#### Newton's Third Law

"To every action there is always opposed an equal reaction."

Less complicated paraphrasing: In the natural world, every action (force) elicits an equal and opposite reaction. When object A applies a force to object B, object B reciprocates with a corresponding and contrasting force on object A. Essentially, forces arise from interactions [41]. In practical terms, the third law enables the addressing of dynamical problems by employing an equilibrium equation.

## Newton's Law of Universal Gravitation

“Two bodies, the masses of which are  $M$  and  $m$ , respectively, attract one another along the line joining them with a force proportional to the product of their masses and inversely proportional to the square of the distance between them.”

Newton enunciated the Law of Universal Gravitation in Equation 3.7, where  $G$  is the universal gravitational constant, equal to  $6.673 \times 10^{-11} \text{ m}^3 \text{ kg}^{-1} \text{ s}^{-2}$  and  $r$  is the mutual distance.

$$F = G \frac{Mm}{r^2} \quad (3.7)$$

## 3.4 Derivation of the Equations of Motion: The Two-Body Problem

After removing complexities, the lunar landing becomes a two-body problem involving the Moon and the LL. The engagement between these two bodies complies with Newton's Laws of Motion and EOMs can be acquired from these interactions.

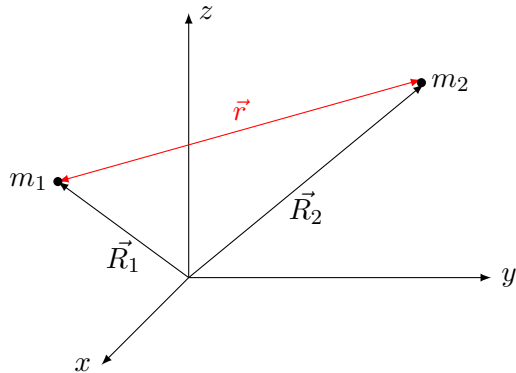


Figure 3.5: Two-body system in an inertial frame of reference.

Take into account a system consisting of two spherically symmetric bodies with masses  $m_1$  and  $m_2$ , where  $m_1$  is greater than  $m_2$ , interacting only through gravitational forces. Within an inertial frame  $\mathcal{F}_i$  (Figure 3.5), vectors  $\vec{R}_1$  and  $\vec{R}_2$  represent the positions of masses  $m_1$  and  $m_2$ , respectively. The relative position of  $m_2$  with respect to  $m_1$  can be defined as in Equation 3.8 [5]. Their mutual distance is  $r = \|\vec{r}\|$  and Equations 3.9 and 3.10 apply to the relative velocity and acceleration.

$$\vec{r} = \vec{R}_2 - \vec{R}_1 \quad (3.8)$$

$$\dot{\vec{r}} = \dot{\vec{R}}_2 - \dot{\vec{R}}_1 \quad (3.9)$$

$$\ddot{\vec{r}} = \ddot{\vec{R}}_2 - \ddot{\vec{R}}_1 \quad (3.10)$$

The force acting on each mass is determined by the Law of Universal Gravitation (Equation 3.7). This allows the independent description of each mass's motion using the second law of dynamics (Equation 3.5) through Equations 3.11 and 3.12. By subtracting the second equation from the first and applying a straightforward simplification related to the masses, one attains Equation 3.13.

$$m_1 \ddot{\vec{R}}_1 = G \frac{m_1 m_2}{r^3} \vec{r} \quad (3.11)$$

$$m_2 \ddot{\vec{R}}_2 = -G \frac{m_1 m_2}{r^3} \vec{r} \quad (3.12)$$

$$\ddot{\vec{r}} = -G \frac{m_1 + m_2}{r^3} \vec{r} \quad (3.13)$$

In most practical scenarios, one mass greatly exceeds the other. Specifically, for the Moon and the LL,  $m_1$  designates the mass of the Moon ( $M$ ) and  $m_2$  denotes the mass of the LL ( $m$ ), with  $m_1 \gg m_2$ .

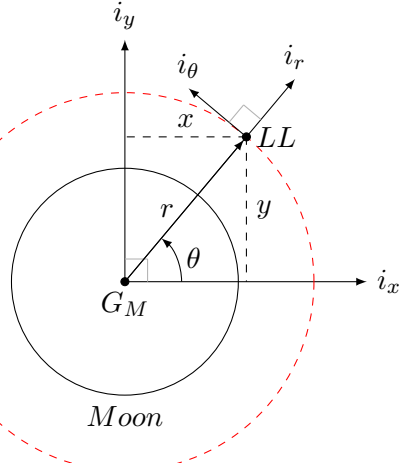


Figure 3.6: Non-rotating and orbit frames.

This adjustment simplifies the EOM (Equation 3.13) into the more manageable form given by Equation 3.14, where  $\mu$ , equivalent to  $GM$ , represents the gravitational parameter of the primary body.

$$\ddot{\vec{r}} = -\frac{\mu^3}{r^3} \vec{r} \quad (3.14)$$

A rotating frame  $\mathcal{F}_0$  is positioned around the spacecraft, allowing velocity and acceleration components to be defined in the frame depicted in Figure 3.6, as articulated in Equations 3.15 and 3.16. By computing the time derivative, one obtains Equations 3.17 and 3.18.

$$\hat{i}_r = \cos(\theta) \hat{i}_x + \sin(\theta) \hat{i}_y \quad (3.15)$$

$$\hat{i}_\theta = -\sin(\theta) \hat{i}_x + \cos(\theta) \hat{i}_y \quad (3.16)$$

$$\dot{\hat{i}}_r = \dot{\theta} \hat{i}_\theta \quad (3.17)$$

$$\dot{\hat{i}}_\theta = -\dot{\theta} \hat{i}_r \quad (3.18)$$

The description of the position vector is displayed in Equation 3.19, while the velocity vector is portrayed in Equation 3.20, which includes its radial velocity  $v_r$  and tangential velocity  $v_\theta$ .

$$\vec{r} = r \hat{i}_r \quad (3.19)$$

$$\vec{v} = v_r \hat{i}_r + v_\theta \hat{i}_\theta \quad (3.20)$$

Upon calculating the first derivative of the position vector (Equation 3.19) and the velocity vector (Equation 3.20), one derives Equations 3.21 and 3.22.

$$\vec{v} = \frac{d\vec{r}}{dt} = \frac{d}{dt}(r\hat{i}_r) = \dot{r}\hat{i}_r + r\dot{\hat{i}}_r = \dot{r}\hat{i}_r + r\dot{\theta}\hat{i}_\theta \quad (3.21)$$

$$\vec{a} = \frac{d\vec{v}}{dt} = \frac{d^2\vec{r}}{dt^2} = (\ddot{r} - r\dot{\theta})\hat{i}_r + (r\ddot{\theta} + 2\dot{r}\dot{\theta})\hat{i}_\theta \quad (3.22)$$

The radial and tangential components of Equation 3.21 are expressed in Equations 3.23 and 3.24. Equation 3.22 supplies the radial and tangential components of the acceleration vector, as shown in Equations 3.25 and 3.26.

$$v_r = \dot{r} \quad (3.23)$$

$$v_\theta = r\dot{\theta} \quad (3.24)$$

$$a_r = \ddot{r} - r\dot{\theta} \quad (3.25)$$

$$a_\theta = r\ddot{\theta} + 2\dot{r}\dot{\theta} \quad (3.26)$$

According to [5], in addition to the gravity pull from the primary body, the spacecraft also encounters other forces, such as gravitational perturbations caused by other celestial bodies and thrust generated by the engine for orbit modification. Disregarding other perturbations and assuming that the spacecraft's motion is directed by an engine generating an acceleration  $\vec{a}_T$  at an angle  $\psi$  from the radial direction, the vector EOM can be written as in Equation 3.27. This can then be decomposed into its radial and tangential components using Equation 3.25 and Equation 3.26, resulting in Equations 3.28 and 3.29.

$$\ddot{r} = -\frac{\mu}{r^3}\vec{r} + \vec{a}_T \quad (3.27)$$

$$a_r = -\frac{\mu}{r^2} + a_T \cos \psi \quad (3.28)$$

$$a_\theta = a_T \sin \psi \quad (3.29)$$

The spacecraft pitch angle  $\psi$  is represented as the counterclockwise angle between the ac-

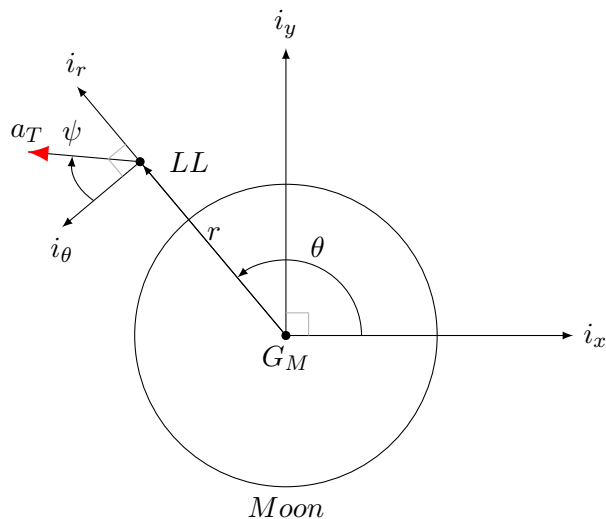


Figure 3.7: The LL in the frame of reference.

celeration vector  $\vec{a}_T$  and the axis  $i_\theta$ , as illustrated in Figure 3.7. As indicated by [12], the acceleration vector can be defined as presented in Equation 3.30. Here,  $T_{\max}$  denotes the maximum engine thrust,  $k_E$  is a throttle command utilised to alter the engine's power output and  $m$  stands for the LL's mass. Bearing in mind Equations 3.31 and 3.32, one can derive the set of first-order ordinary differential equations that explain how the spacecraft's state changes over time. These are detailed in the next section.

$$\vec{a}_T = \frac{T_{\max}k_E}{m} \quad (3.30)$$

$$v_r = \dot{r} \Rightarrow \dot{v}_r = \ddot{r} \quad (3.31)$$

$$v_\theta = r\dot{\theta} \Rightarrow \dot{v}_\theta = \dot{r}\dot{\theta} + r\ddot{\theta} \quad (3.32)$$

### 3.5 Finalised Equations of Motion

This section is heavily influenced by [12] and the following equations are employed to compute the optimal descent trajectory. In Figure 3.8, radial and tangential components are depicted to better visualise how the velocities affect the spacecraft.

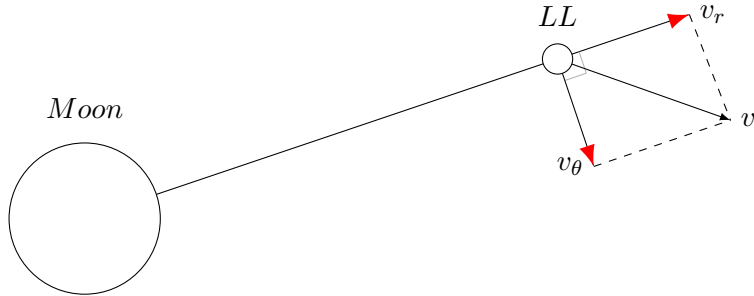


Figure 3.8: Radial and tangential velocity.

#### Translational Dynamics

The vehicle's position in polar coordinates is defined by  $r$ , the distance from the centre of the main body and the central angle  $\theta$ , measured from the inertial  $x$ -axis. The velocity comprises radial  $v_r$  and tangential  $v_\theta$  components. The mentioned quantities can be seen in Figure 3.8. With  $\psi$  referring to the angle between the thrust vector and the radius vector, the translational dynamics follow Equations 3.33–3.36.

$$\dot{r} = v_r \quad (3.33)$$

$$\dot{\theta} = \frac{v_\theta}{r} \quad (3.34)$$

$$\dot{v}_r = \frac{v_\theta^2}{r} - \frac{\mu}{r^2} + \frac{T_{\max}k_E}{m} \cos \psi \quad (3.35)$$

$$\dot{v}_\theta = -\frac{v_r v_\theta}{r} + \frac{T_{\max}k_E}{m} \sin \psi \quad (3.36)$$

The acceleration resulting from the applied thrust is described by the expressions involving trigonometric functions in the last two EOMs. Furthermore,  $v_\theta^2/r$  and  $-\mu/r^2$ , as found in Equation 3.35, correspond to the centrifugal and gravitational terms, respectively.

## Rotational Kinematics

The spacecraft revolves around an axis perpendicular to the plane of translational movement. Therefore, simplifying the rotational EOMs involves regulating the rate of change of inertial angular velocity  $\omega$  by controlling inertial angular acceleration  $\alpha$ . Equations 3.37–3.38 are in polar coordinates.

$$\dot{\psi} = \omega - \dot{\theta} = \omega - \frac{v_\theta}{r} \quad (3.37)$$

$$\dot{\omega} = \alpha \quad (3.38)$$

## Variable Mass

Upon ignition of either the thrusters or the engine, the vehicle's mass diminishes. Equation 3.39 represents the comprehensive mass flow equation. The lower indexes  $\square_J$  and  $\square_E$  differentiate between quantities related to the reaction control system (RCS) and the engine.

$$\dot{m} = -\frac{T_{\max E} k_E}{V_{exE}} - \frac{T_{\max J}}{V_{exJ}} \sum_{i=1}^{N_J} k_i \quad (3.39)$$

The equation, accounting for variable mass, resembles Equation 3.39 but excludes the mass flow from the thrusters. Since the mass flow due to the engine is notably greater than the aggregate mass flow due to the RCS firing, the previous assumption appears plausible. Section 4.2 will explore an indirect approach to address the reduction of mass caused by RCS thrusters. The final calculation of mass flow is provided in Equation 3.40.

$$\dot{m} = -\frac{T_{\max E} k_E}{V_{exE}} \quad (3.40)$$

## Chapter 4

# Optimal Descent Trajectory

This chapter focuses on computation of the optimal descent trajectory. It begins with an explanation of optimisation problem theory and methods for solving them. This is followed by an introduction to the used optimisation software, Bocop. Finally, the chapter concludes with a description of the problem's implementation and its results.

### 4.1 Optimisation Problem Theory

Numerous applied problems frequently involve seeking the most efficient solution, often entailing maximising or minimising a function. This could mean minimising travel time or minimising costs for a given task, or maximising the power output of a device. Calculus techniques are commonly employed to address such challenges. By identifying the appropriate function and applying calculus methodologies, many of these problems can be resolved to ascertain the desired maximum or minimum value.

In mathematical terms, these problems are typically formulated as determining the maximum or minimum value of  $f(x)$  within a defined interval  $a \leq x \leq b$ . While sometimes  $a$  or  $b$  may extend to infinity, real-world constraints regularly limit the possible values of  $x$ . This varies from relative maximum and minimum problems encountered when graphing functions in two ways: our focus is solely on the function's behaviour within the interval  $a$  to  $b$  and our objective is to find the largest or smallest value that  $f(x)$  attains, not just locating local extremes. In other words, our interest lies in uncovering global (or absolute) maximum or minimum values, rather than relative ones [10].

#### Optimisation Problem Statement

Formally, an optimisation problem can be articulated as:

Given a function  $f$  that maps a set  $X$  to totally ordered set  $Y$ , determine the optimal element  $x^* \in X$  such that  $f(x^*) \leq f(x)$  for all  $x \in X$ .

Mathematicians favour brevity, so the problem is frequently reformulated to avoid verbosity. Thus, it is common to express the above statement as Equation 4.1 and the optimal choices  $x^*$  is usually denoted as shown in Equation 4.2.

$$\min f(x) \tag{4.1}$$

$$x^* = \operatorname{argmin}_x f(x) \tag{4.2}$$

In simpler terms, this refers to the argument that minimises the function. Our choice of the inequality  $\leq$  in the definition is not particularly unique. Several optimisation textbooks utilise the convention  $\geq$ ,  $\max$  and  $\operatorname{argmax}$  to establish their optimisation framework. It is important to note that this choice does not impact the generality of the problem. A canonical transformation  $f \rightarrow -f$ , which transforms  $f(x) \rightarrow -f(x) \forall x$ , converts the minimisation of  $f$  into the maximisation of  $-f$  [35].

## Objective Function

For a globally convex function (which rises monotonically in every direction from the global optimum), any local optimum discovered will also serve as the global optimum, representing either the maximum or minimum value of the objective function. From here, we will substitute “optimum” with “minimum”. However, in the case of a nonconvex function, identifying a local minimum does not guarantee that it is the global minimum. Figure 4.1 portrays the differences between convex and nonconvex functions, as well as local and global minima, for an arbitrary one-dimensional function  $f(x)$ .

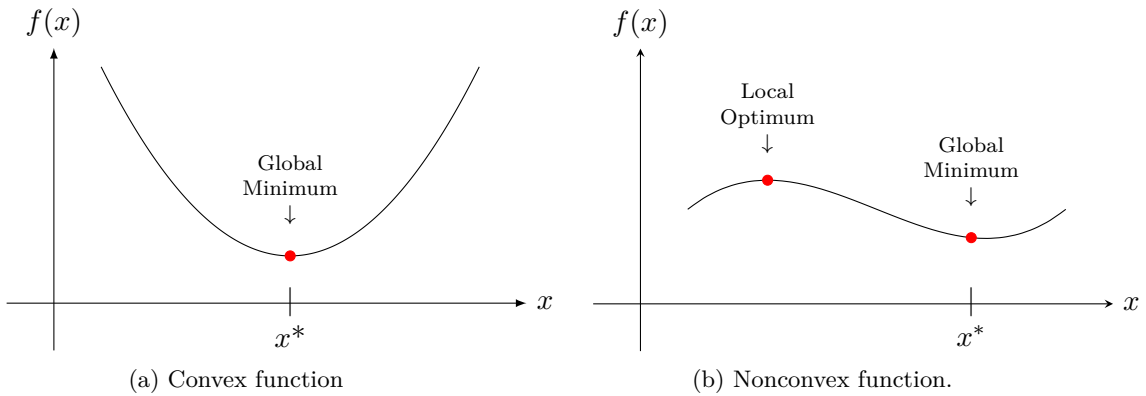


Figure 4.1: One-dimensional convexity.

For a convex example, the global minimum is the only optimal solution. In the instance of the nonconvex function we are considering, there are two optimal solutions: one being a local optimum and the other the global minimum. Since most trajectory optimisation problems are nonconvex, solely local minima are found with ease [12].

## Finding a Minimum

To find a local minimum of a single-variable function  $f(x)$ , locate a point where the first derivative of the function is zero and the second derivative is positive. The first derivative of the function  $f(x)$ , designated as  $f'(x)$  or  $\frac{df}{dx}$ , is the slope of the tangent line to the function at the point  $x$ . A zero slope does not provide definitive information about the function’s behaviour; at that point, the function could be increasing, decreasing or could correspond to a local maximum or minimum. By expressing this in terms of derivatives, we can observe that:

- if  $f'(q) = 0$ , then  $x = q$  is referred to as a critical point of  $f(x)$  and this reveals no additional information about the nature of  $f(x)$  at  $x = q$ ,
- or  $f'$  does not exist at  $q$ .

We frequently use the second derivative of the function, known as the *Second Derivative Test*, to ascertain whether  $x$  is a local maximum or a local minimum. If  $x$  is a critical point and the second derivative at that point is positive, this indicates that the first derivative of  $f(x)$  is increasing at  $x$  and the graph of the function is concave up at that point. In this scenario, where the slope of the function is zero and the graph is concave up, the point must be a local minimum [6]:

- if  $f'(q) = 0$  and  $f''(q) > 0$ , then  $f(x)$  has a local minimum at  $x = q$ .

According to [29], this test is extended to multivariable functions as follows: initially, we construct the *Hessian* matrix, which contains the second partial derivatives evaluated at  $q$ . For a function  $f$  with  $n$  variables, the Hessian is an  $n \times n$  matrix  $H$ , where each entry in row  $k$ , column  $l$  of  $H$  is given by Equation 4.3.

$$H_{kl} = \frac{\partial^2 f(q)}{\partial x_k \partial x_l}. \quad (4.3)$$

The *Second Derivatives Test* can be articulated in this manner: A point  $q$  is a local minimum of the function  $f$  if it is a critical point and the Hessian matrix  $H$  at  $q$  is positive definite. For a symmetric matrix  $H$ , several conditions are equivalent:  $H$  is positive definite, all the eigenvalues of  $H$  are positive, the determinant of  $H$  is positive and so on.

## Optimal Control Problem

The issue of identifying the best descent trajectory is a type of optimisation problem known as an OCP. This area of study focuses on optimising controlled dynamical systems. In a controlled dynamical system, the trajectory can be continuously modified over time by selecting a control parameter  $z(t)$ . Such a system is typically characterised by ordinary differential equations outlined in Equation 4.4 and 4.5.

$$\dot{x}(t) = f(t, x(t), z(t)), t > 0 \quad (4.4)$$

$$x(t_i) = x_{t_i} \in \mathbb{R}^d \quad (4.5)$$

In this context,  $z : \mathbb{R}^d \rightarrow Z$  signifies the control function, with  $Z$  being an appointed set referred to as the control set, as described in Equation 4.6.

$$f : \mathbb{R}_+ \times \mathbb{R}^d \times Z \rightarrow \mathbb{R}^d \quad (4.6)$$

Selecting the value of  $z(t)$  enables control over the state trajectory  $x(t)$ . For the optimal descent trajectory,  $z(t)$  functions as a control parameter, managing the thrust of the LL engine. The challenge is to determine a sequence of rocket thrust values that minimise the objective function  $\mathcal{J}$  (see Equation 4.7), where  $c$  represents the cost function and  $t_i$  and  $t_f$  mark the start and end times, respectively [11].

$$\mathcal{J} = \int_{t_i}^{t_f} c(t, x(t), z(t)) dt \quad (4.7)$$

## Methods for Solving Optimal Control Problems

For the majority of non-linear OCPs, finding analytical solutions is often extremely difficult, if not unfeasible. Consequently, researchers have adopted numerical techniques and computational tools to discover optimal solutions. These numerical approaches are generally divided into two primary categories: direct and indirect.

An indirect method relies on the costate differential equations, the maximum principle and boundary conditions to determine the optimal solution. An a priori estimate of the costate is necessary for this method, which can be problematic due to the costate's frequent lack of direct physical interpretation.

In contrast, a direct method focuses on optimising the cost function immediately, is the more commonly used approach. This method begins with an initial estimate for the state and control, then scans within the feasible region to locate the minimum cost function value. It typically results in a local minimum solution since exploring the entire feasible region is often impractical. However, if the problem is convex, achieving local optimality also ensures global optimality.

Given that users are usually more knowledgeable about the problem's dynamics, providing an initial guess for the state and control is simpler than approximating the costate [12]; hence, the direct method was chosen for this thesis.

### Midpoint Method

In this work, the OCP solver offers various methods for solving differential equations. The midpoint method was chosen for its ability to produce the best results within an acceptable computation time.

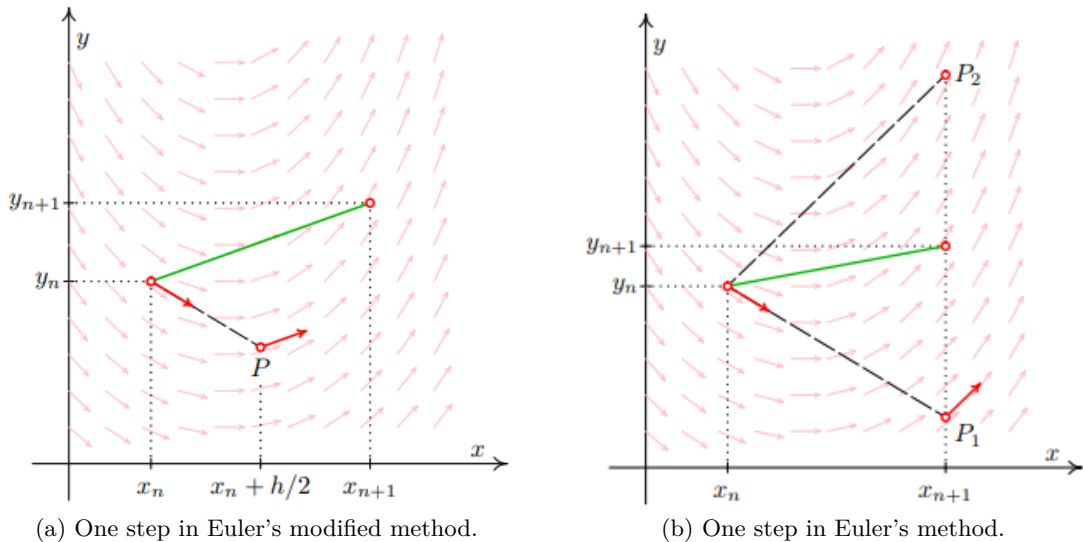


Figure 4.2: Midpoint method. Source: [8].

The midpoint method, illustrated in Figure 4.2 (a), is a modification of Euler's method and is a one-step technique, utilising information only from the preceding step to determine the new state. It is designed to resolve the differential equation presented in Equation 4.8.

$$y' = f(x, y), \quad y(x_0) = y_0 \quad (4.8)$$

The (explicit) computation of  $y_{i+1}$  is given by the formula shown in Equations 4.9–4.11, where  $h$  is step size and  $i = 0, \dots, n - 1$ . The implicit midpoint method, depicted in Figure 4.2 (b), is also referred to as the Euler method.

$$k_1 = f(x_i, y_i) \quad (4.9)$$

$$k_2 = f(x_i + \frac{1}{2}h, y_i + \frac{1}{2}hk_1) \quad (4.10)$$

$$y_{i+1} = y_i + hk_2 \quad (4.11)$$

Starting at the initial point  $[x_n, y_n]$  and using the derivative to determine the slope, a tangent line is extended. A provisional point  $P$  along this line serves as an estimate for the midpoint of the interval,  $x_n + h/2$ . By employing the coordinates of  $P$  to compute the slope at this new point, another tangent line is extended. The intersection of this line with the vertical line at  $x_{n+1}$  yields the next point,  $[x_{n+1}, y_{n+1}]$  [8].

## 4.2 Implementation of Optimal Descent Trajectory

This section provides an overview of the optimisation software and outlines the implementation of the optimal descent trajectory problem.

### Bocop

The purpose of the Bocop project is to create an open-source toolkit specifically designed for addressing optimal control problems. The original package enforces a local optimisation technique to transform the OCP into a finite-dimensional optimisation problem (NLP) through time discretization, known as the direct transcription method. The resulting NLP problem is then tackled using the renowned IPOPT software [1]. We are examining an optimal control problem of the subsequent form:

$$(P) = \begin{cases} \text{Min } J(t_0, y(t_0), t_f, y(t_f), \pi) & \text{Objective} \\ \dot{y}(t) = f(t, u(t), y(t), z(t), \pi) & \text{Dynamics} \\ \Phi_l \leq \Phi(t_0, y(t_0), t_f, y(t_f), \pi) \leq \Phi_u & \text{Boundary conditions} \\ y_l \leq y \leq y_u, u_l \leq u \leq u_u, z_l \leq z \leq z_u, \pi_l \leq \pi \leq \pi_u & \text{Bounds} \\ g_l \leq g(t, u(t), y(t), z(t), \pi) \leq g_u & \text{Path constraints} \end{cases}$$

with  $y(\cdot)$  standing for the state variables,  $u(\cdot)$  denoting the control,  $z(\cdot)$  as the optional algebraic variables and  $\pi$  indicating the variables to be optimised, in contrast to the numerical constants of the problem. According to [1], the problem  $(P)$  is characterised by:

- **4 functions (C / C++)** pertaining to  $J, f, \Phi, g$ :  
**criterion, dynamics, boundarycond** and **pathcond**. Each one of these functions is stored in a `.tpp` file and can be edited with any text editor as needed.
- **3 definition files in unformatted text:**
  - `problem.def` for overall definition and configurations
  - `problem.bounds` regarding the limits
  - `problem.constants` holds the optional constant values relevant to the problem

Each problem is organised in its own directory, containing all related files. Generally, these files are produced via the GUI, which facilitates the creation, loading and saving of problems. Advanced users may opt to edit the `.def`, `.bounds` and `.constants` files manually.

## Bocop GUI

The Bocop interface is designed with a user-friendly GUI developed with the Qt framework and is structured into four major modules [1]:

- *Definition:* Define the optimal control problem by specifying the variable dimensions and names, as well as the functions for the objective, dynamics and constraints. Recompilation is required only when modifying one of the functions. The module involves selecting the discretization method and the number of steps to convert the OCP into a nonlinear programming issue. One can utilise various implicit Runge-Kutta methods, including predefined options such as Euler, Midpoint, RK4, Gauss and Lobatto formulas.
- *Starting Point:* Set the initial point of the discretized NLP problem at iteration 0. Since the nonlinear programming solver relies on a local method, convergence may strongly depend on an advantageous starting position. Bocop provides a graphical interface to generate initial trajectories, offering options like constant, piecewise linear, spline functions or external files.
- *Optimisation:* Clicking the “Optimise“ button initiates IPOPT to tackle the discretized optimisation problem. Users can adjust options for the NLP solver IPOPT, with these settings being saved in a standard configuration file named `ipopt.opt`. Furthermore, this tab offers optional features such as batch optimisation, parameter identification and selecting an existing solution as the starting point.
- *Visualisation:* Read and display the solution file generated after optimisation. The visualisation encompasses state and control variables, scalar optimisation parameters like free final time and constraints, including dynamic constraints and their associated multipliers.

Figure 4.3, shows a screenshot of Bocop’s primary window.

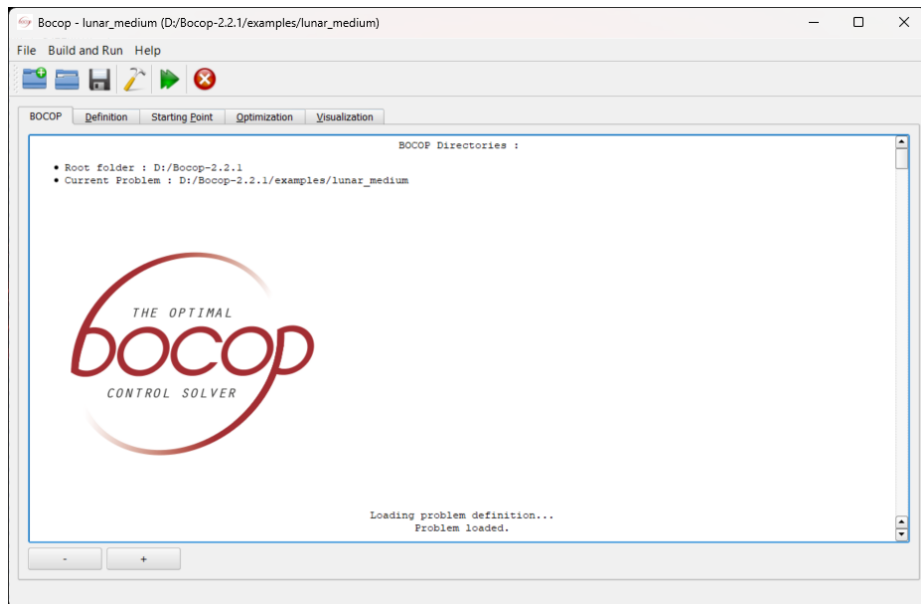


Figure 4.3: Main window of the Bocop GUI.

## The Problem Implementation in Bocop

The following section delves into the matter of the optimal descent trajectory, implemented in Bocop. When working with Bocop, the first step is to specify the name and number of dimensions for each variable. The seventh-dimensional state vector is expressed in Equation 4.12, where  $r$  stands for the distance from the Moon to the LL,  $\theta$  denotes the central angle,  $v_r$  and  $v_\theta$  are the radial and tangential velocity,  $\psi$  symbolises the spacecraft's pitch angle,  $\omega$  indicates the angular velocity and  $m$  signifies the spacecraft's mass.

$$y(t) = [r(t), \theta(t), v_r(t), v_\theta(t), \psi(t), \omega(t), m(t)] \quad (4.12)$$

The two-dimensional control vector is defined in Equation 4.13 and is composed of the engine throttle command and angular acceleration, in that sequence. Boundary conditions and constants vary across diverse parts of the trajectory and will be covered later.

$$u(t) = [k_E(t), \alpha(t)] \quad (4.13)$$

## Trajectory Division

As discussed in Section 2.4, the trajectory is segmented into four phases: *Rough Braking*, *Attitude Hold*, *Fine Braking* and *Terminal Descent*. To calculate the optimal trajectory, the problem is divided into these four phases by incorporating three knots. One knot is positioned near the end of the *Rough Braking Phase*, the second at the conclusion of the *Attitude Hold Phase* and the third close to the beginning of the *Fine Braking Phase*. However, the precise placement of each knot is adjustable and determined by the optimiser. State equality at knot locations is enforced through event constraints, while allowing for discontinuity in control. The bounds on the control variables and events are inspired by [12] and are documented below. Variables  $t_i$  and  $t_f$  represent the initial and final times, respectively. Meanwhile,  $t_1$ ,  $t_2$  and  $t_3$  serve as the first, second and third time stamps in the trajectory division, in this order.

## Control Variable Constraints

According to [12], to prevent engine restart failures, it is recommended to maintain continuous thrust throughout the braking burn, particularly during the *Rough Braking* and *Fine Braking Phases* of our study. Consequently, a continuous burn was imposed by constraints that keep the vehicle throttle above its minimum threshold. In the *Attitude Hold Phase*, there is an unrestricted throttle limit to preserve the current attitude. During the *Terminal Descent*, the throttle could fluctuate within its open range to accommodate free-fall trajectories. This approach was based on [12], which found that the minimum fuel solution involved allowing the vehicle to free fall until maximum thrust was exerted. The appointed maximum angular acceleration limit aligns with estimates detailed in [12].

$$\text{Rough Braking Phase} \quad 0.4 \leq k_E(t) \leq 1 \quad \text{for } t_i \leq t \leq t_1 \quad (4.14)$$

$$\text{Attitude Hold Phase} \quad 0 \leq k_E(t) \leq 1 \quad \text{for } t_1 \leq t \leq t_2 \quad (4.15)$$

$$\text{Fine Braking Phase} \quad 0.4 \leq k_E(t) \leq 1 \quad \text{for } t_2 \leq t \leq t_3 \quad (4.16)$$

$$\text{Terminal Descent Phase} \quad 0 \leq k_E(t) \leq 1 \quad \text{for } t_3 \leq t \leq t_f \quad (4.17)$$

$$\text{All phases} \quad -0.5^\circ \text{ s}^{-2} \leq \alpha(t) \leq 0.5^\circ \text{ s}^{-2} \quad \text{for } t_i \leq t \leq t_f \quad (4.18)$$

## Event Constraints

Equations 4.19—4.21 define the state at the knot, with  $\square^-$  and  $\square^+$  indicating the state values immediately before and after the knot, in this succession. Equation 4.22 secures the sequential progression of events.

$$m^-(t_1) = m^+(t_1) \quad (4.19)$$

$$m^-(t_2) = m^+(t_2) \quad (4.20)$$

$$m^-(t_3) = m^+(t_3) \quad (4.21)$$

$$t_i < t_1 < t_2 < t_3 < t_f \quad (4.22)$$

## Constants

The constants are laid out in Table 4.1, with data taken from [9, 40].  $T_{\max}$  is the maximum thrust of the LL, which is 740 N per engine, with four engines engaged during the *Rough Braking, Attitude Hold* and *Fine Braking Phases*. In [47], P. Veeramuthuvel, a project director of Chandrayaan-3, stated that throughout the entire *Terminal Descent Phase*, only two of the four engines continued firing while the other two were shut off, thereby halving the maximum thrust compared to the other phases.  $V_{ex}$  represents the engine exhaust velocity and it is computed as shown in Equation 4.23, where  $I_{sp}$ , the specific impulse of the spacecraft engines, is equal to 310 s and  $g_E$  designates the gravitational acceleration of the Earth ( $9.8 \text{ m s}^{-2}$ ).

$$V_{ex} = I_{sp} \cdot g_E \quad (4.23)$$

$V_{ex}$  remains unchanged because it is a fundamental property of the engine, primarily determined by its  $I_{sp}$  and  $g_E$ . This characteristic velocity stays consistent regardless of whether the engine operates at full or reduced thrust.  $R_{eq}$  denotes the Moon's equatorial radius and  $\mu$  stands for its gravitational parameter. The EOMs are based on radians, so all measured in degrees were converted accordingly.

Table 4.1: Constant values used in the optimal descent trajectory.

Constant	Rough Braking, Attitude Hold and Fine Braking Phases	Terminal Descent Phase
$T_{\max}$	2 960 N	1 480 N
$V_{ex}$		$3 038 \text{ Ns kg}^{-1}$
$R_{eq}$		$1.7381 \times 10^6 \text{ m}$
$\mu$		$4.902800076 \times 10^{12} \text{ m}^3 \text{ s}^{-2}$

## Initial Mass

An official detailed report of the Chandrayaan-3 mission is currently unavailable on the internet. Consequently, our initial mass estimation will rely on the results from the previous mission, Chandrayaan-2. The rationale behind this approach is straightforward: the space agency opted for a failure-based design strategy in Chandrayaan-3, in contrast to the success-based design of Chandrayaan-2. This implies that even in the event of multiple failures, the spacecraft should still achieve a soft landing. Additionally, Chandrayaan-3

incorporated the original LL and Rover from Chandrayaan-2, albeit with slight modifications to enhance the likelihood of a successful touchdown. Furthermore, considering that both missions involved identical sequences of events, including launch, 5 EBNs, TLI, 5 LBNs, separation, 2 DEOs and landing, the obtained result should not deviate significantly from the truth.

After a series of firings by the PM, the Lander attained a polar lunar orbit at an altitude of  $153 \text{ km} \times 163 \text{ km}$  by 17 August. Subsequently, the Vikram Lander, with a mass of 1 749.86 kg, inclusive of 26 kg for the Rover [38], separated. Two DEOs were performed, as detailed in [32]: the first DEO consumed 1.50 kg of propellant, followed by the second DEO which utilised 11.3 kg of fuel. Both Chandrayaan-2 and Chandrayaan-3 began their power descent from an approximate altitude of 30 km. Taking these factors into account, we can estimate our initial mass to be 1 737.06 kg.

## State Variable Bounds

Restrictions on state variables are crucial for the mission, ensuring that not a single variable reaches an invalid value during the flight. These boundaries persist invariant across all phases of the mission. To restrict the rotational motion of the Lander to reasonable levels, the limits on angular velocity were set in compliance with [12]. Given that the centre of the Moon's gravity serves as the reference point for  $r$ , zero altitude corresponds to the lunar equatorial radius, marking the lower bound. It is also important to note that the upper bound for altitude is calculated by adding the starting altitude of 30 km to the Moon's radius. The central angle is constrained to  $180^\circ$  to guarantee that the spacecraft remains above the ground, covering directions from the reference point up to half of the circle.

The spacecraft is intended for descent, so the radial velocity is capped at  $0 \text{ m s}^{-1}$ , while the lower bound for tangential velocity is fixed at  $0 \text{ m s}^{-1}$  to establish forward movement. The range for the  $\psi$  angle symbolises the LL pitch, spanning from  $-90^\circ$  to  $0^\circ$ . This indicates that the spacecraft commences its descent from a horizontal position and aims to transition to a vertical position by the end of the manoeuvre. The vehicle's weight must exceed its dry mass. Each boundary condition needs to be linked to certain state variables, so the `boundarycond.tpp` file is complete. The bounds can be seen in next Table 4.6:

Table 4.2: State variable bounds of the problem.

Variable	Lower Bound	Upper Bound
$r(t)$	1 738 100 m	1 768 100 m
$\theta(t)$	$0^\circ = 0 \text{ rad}$	$180^\circ = 3.14159265 \text{ rad}$
$v_r(t)$	—	$0 \text{ m s}^{-1}$
$v_\theta(t)$	$0 \text{ m s}^{-1}$	—
$\psi(t)$	$-90^\circ = -1.57079633 \text{ rad}$	$0^\circ = 0 \text{ rad}$
$\omega(t)$	$-10^\circ \text{ s}^{-1} = -0.174532925 \text{ rad s}^{-1}$	$10^\circ \text{ s}^{-1} = 0.174532925 \text{ rad s}^{-1}$
$m(t)$	707.48 kg	1 737.06 kg

## Initial and Final Conditions

Commencing and terminal conditions differ for every phase of the powered descent, thus the trajectory is individually described for each segment below. To ensure a seamless

transition between phases and because each phase requires separate computation, the final conditions of each phase will serve as the initial conditions for the subsequent phase.

### Rough Braking Phase

The descent starts at an elevation of 30 km over the surface.  $\theta(t_i)$  is set to  $-90^\circ$ , which is chosen as a precautionary measure to allow movement in both directions, effectively positioning it midway between  $0^\circ$  and  $180^\circ$ . In circular motion, the object's position remains fixed at a consistent distance from the centre of motion, resulting in no radial velocity. As claimed by [55], the tangential velocity should be  $1\,680 \text{ m s}^{-1}$ . The pitch angle of the vehicle is set to  $-90^\circ$ . The spacecraft's weight aligns with the value outlined in Subsection 4.2. The objective of this phase is to reduce the altitude by 22.6 km and decrease the velocity by  $61 \text{ m s}^{-1}$  vertically and  $1322 \text{ m s}^{-1}$  horizontally.

Table 4.3: Initial and final conditions for Rough Braking Phase

Variable	Initial Values for $t_i$	Final Values for $t_1$
$r(t)$	1 768 100 m	1 745 500 m
$\theta(t)$	$90^\circ = 1.570796327 \text{ rad}$	—
$v_r(t)$	$0 \text{ m s}^{-1}$	$-61 \text{ m s}^{-1}$
$v_\theta(t)$	$1\,680 \text{ m s}^{-1}$	$358 \text{ m s}^{-1}$
$\psi(t)$	$-90^\circ = -1.57079633 \text{ rad}$	—
$\omega(t)$	$0^\circ \text{ s}^{-1} = 0 \text{ rad s}^{-1}$	—
$m(t)$	1 737.06 kg	—

### Attitude Hold Phase

Maintaining a constant pitch angle is the primary goal of the current phase, therefore, the final conditions are slightly adjusted to include an extra constraint for  $\psi(t_2)$ . Additionally, the height above the surface has diminished by 0.6 km, with both radial and tangential speeds lessened by  $2 \text{ m s}^{-1}$  and  $22 \text{ m s}^{-1}$ , respectively.

Table 4.4: Initial and final conditions for Attitude Hold Phase

Variable	Initial Values for $t_1$	Final Values for $t_2$
$r(t)$	1 745 500 m	1 744 900 m
$\theta(t)$	$114.2008018^\circ = 1.99318 \text{ rad}$	—
$v_r(t)$	$-61 \text{ m s}^{-1}$	$-59 \text{ m s}^{-1}$
$v_\theta(t)$	$358 \text{ m s}^{-1}$	$336 \text{ m s}^{-1}$
$\psi(t)$	$-51.86041539^\circ = -0.905135 \text{ rad}$	$-51.86041539^\circ = -0.905135 \text{ rad}$
$\omega(t)$	$0.063954598^\circ \text{ s}^{-1} = 0.0483869 \text{ rad s}^{-1}$	—
$m(t)$	1 074.04 kg	—

### Fine Braking Phase

The aim of the second braking burn is to nullify the velocity and prepare the vehicle for landing. Achieving a near-zero vertical attitude in a legs-down position is essential.

As mentioned in Subsection 2.4, the designated altitude is 1 300 m; hence, the vehicle descended an additional 5.5 km. To optimise conditions for a soft landing,  $\psi(t_3)$  must be nearly vertical. Similarly,  $\omega(t_3)$  should ideally be zero to secure minimal rotational speed.

Table 4.5: Initial and final conditions for Fine Braking Phase

Variable	Initial Values for $t_2$	Final Values for $t_3$
$r(t)$	1 744 900 m	1 739 400 m
$\theta(t)$	$114.3153934^\circ = 1.99518 \text{ rad}$	—
$v_r(t)$	$-59 \text{ m s}^{-1}$	$0 \text{ m s}^{-1}$
$v_\theta(t)$	$336 \text{ m s}^{-1}$	$0 \text{ m s}^{-1}$
$\psi(t)$	$-51.86041539^\circ = -0.905135 \text{ rad}$	$[-0.5^\circ, 0.5^\circ] = [-0.008726646 \text{ rad}, 0.008726646 \text{ rad}]$
$\omega(t)$	$1.431107204^\circ \text{ s}^{-1} = 1.08275 \text{ rad s}^{-1}$	$0^\circ \text{ s}^{-1} = 0 \text{ rad s}^{-1}$
$m(t)$	1 064.24 kg	—

### Terminal Descent Phase

To complete the descent, the radius condition ensures the spacecraft safely lands on the ground, requiring minimal radial velocity and near-zero tangential velocity for a soft landing. Due to convergence issues arising from the imposition of the equality constraint, the radial velocity constraints are eased. Likewise, a pitch angle interval between  $-0.5^\circ$  and  $0.5^\circ$  is deemed suitable for achieving a near-vertical landing. Guaranteeing a zero angular rate upon landing prevented the vehicle from rotating further after impact.

Table 4.6: Initial and final conditions for Terminal Descent Phase

Variable	Initial Values for $t_3$	Final Values for $t_f$
$r(t)$	1 739 400 m	1 738 100 m
$\theta(t)$	$115.1519117^\circ = 2.00978 \text{ rad}$	—
$v_r(t)$	$0 \text{ m s}^{-1}$	$\leq -2 \text{ m s}^{-1}$
$v_\theta(t)$	$0 \text{ m s}^{-1}$	$\leq 0.5 \text{ m s}^{-1}$
$\psi(t)$	$-0.500000787^\circ = -0.00872666 \text{ rad}$	$[-0.5^\circ, 0.5^\circ] = [-0.008726646 \text{ rad}, 0.008726646 \text{ rad}]$
$\omega(t)$	$0^\circ \text{ s}^{-1} = 0 \text{ rad s}^{-1}$	$0^\circ \text{ s}^{-1} = 0 \text{ rad s}^{-1}$
$m(t)$	911.986 kg	—

### Objective Function

The goal of this study is to reduce fuel consumption while adhering to predefined operational constraints. Equation 4.24 specifies the cost function as the final vehicle mass, selected due to its clear relationship with fuel usage. Moreover, this cost function must be programmed in `criterion.tpp`.

$$\mathcal{J}_{\min} = -m(t_f) \quad (4.24)$$

During analysis in [12], rapid fluctuations in angular acceleration were observed, causing jagged profiles in angular rate and thrust angle. Though not immediately impacting final

fuel cost, these fluctuations led to substantial errors. In a real system, they could waste fuel, since the thrusters would need to fire rapidly to generate the necessary torques on the vehicle. To address this issue, the cost of angular acceleration was integrated into the minimised cost. This modified cost function, presented in Equation 4.25, uses the square of angular acceleration to avoid discontinuities. To ensure minimal impact on the overall cost, C was assigned a small value  $1 \times 10^4$ . In summary, Equations 3.33—3.40 must be implemented in the `dynamics.tpp` file to define the dynamics, accomplished by coding them in C++ language.

$$\mathcal{J}_{\min} = -m(t_f) + \int_{t_i}^{t_f} C[\alpha(t)]^2 dt \quad (4.25)$$

### 4.3 Results

Across a duration extending beyond 1 020 s, the Chandrayaan-3 Lander executes its calculated optimal descent trajectory with precision. Beginning its descent from an altitude of 30 km, the spacecraft manoeuvres through a series of adjustments to align itself vertically. Throughout this controlled movement, the throttle command remains primarily at maximum, ensuring a smooth landing. As the LL transitions downward, it reaches a final radial velocity of  $-2 \text{ m s}^{-1}$  and maintains a pitch angle of  $0^\circ$  upon touchdown. Despite consuming 896.294 kg of fuel from its initial load of 1 029.58 kg, the spacecraft lands with a surplus of 133.286 kg of unburnt propellant, representing approximately 12.946 % of its total initial fuel. Notably, the vehicle's mass upon landing comfortably exceeds the minimal threshold, underscoring the resounding success of the optimisation process. Comprehensive details regarding each phase are provided in Table 4.7, with all data rounded to five decimal spaces.

Table 4.7: Segmentation of the Computed Optimal Descent Trajectory

Phase	Vertical Distance [km]	Downrange Distance [km]	Duration [s]	$\Delta\theta [^\circ]$	$\Delta m [\text{kg}]$
Rough Braking	22.6	734.145 06	701.537 85	24.200 80	663.020
Attitude Hold	0.6	3.476 20	10.061 29	0.114 59	9.800
Fine Braking	5.5	25.358 88	159.446 14	0.835 95	152.254
Terminal Descent	1.3	0	159.450 47	0	71.220
Total	30.0	762.997 52	1024.582 95	25.151 91	896.294

The Figures 4.4—4.5 depict results generated with the open-source program Gnuplot. Its selection was based on its versatility as a portable, command-line-driven graphing utility, compatible with a wide range of operating systems including Linux, OS/2, MS Windows, macOS, VMS and numerous others [53]. The descent initiates with the *Rough Braking Phase*, followed by the start of the *Attitude Hold Phase* at 701.538 s, the beginning of the *Fine Braking Phase* at 711.599 s and the onset of the *Terminal Descent Phase* at 871.045 s. Each of the four phases is highlighted with alternating shades of grey,

switching between two different shades. The commencing values for each phase, which are also the terminal values for the previous phase, are shown through horizontal dotted lines. Downrange distance is estimated as the product of the difference in central angle and the radius of the Moon, yielding a value equal to 762.997 52 km. It is shown in Figure 4.4 (a). In Figure 4.4 (b), we present the optimal descent trajectory altitude navigating over time. Moving to Figure 4.4 (c), one can track the Lander's central angle progression. Figure 4.4 (d) monitor the LL's pitch angle over time, gradually transitioning from  $-90^\circ$  to  $0^\circ$ . Figure 4.5 (a) illustrates the radial velocity of the LL, peaking at  $-67.19 \text{ m s}^{-1}$ . Tangential velocity can be observed in Figure 4.5 (b). Figure 4.5 (c) portrays the LL's mass dynamics throughout the power descent. Figure 4.5 (d) elucidates the throttle command applied to the LL's engine over time, predominantly kept at maximum throughout the landing manoeuvre. Finally, in Figures 4.5 (e) and 4.5 (f) one can see the angular velocity and acceleration, in this sequence.

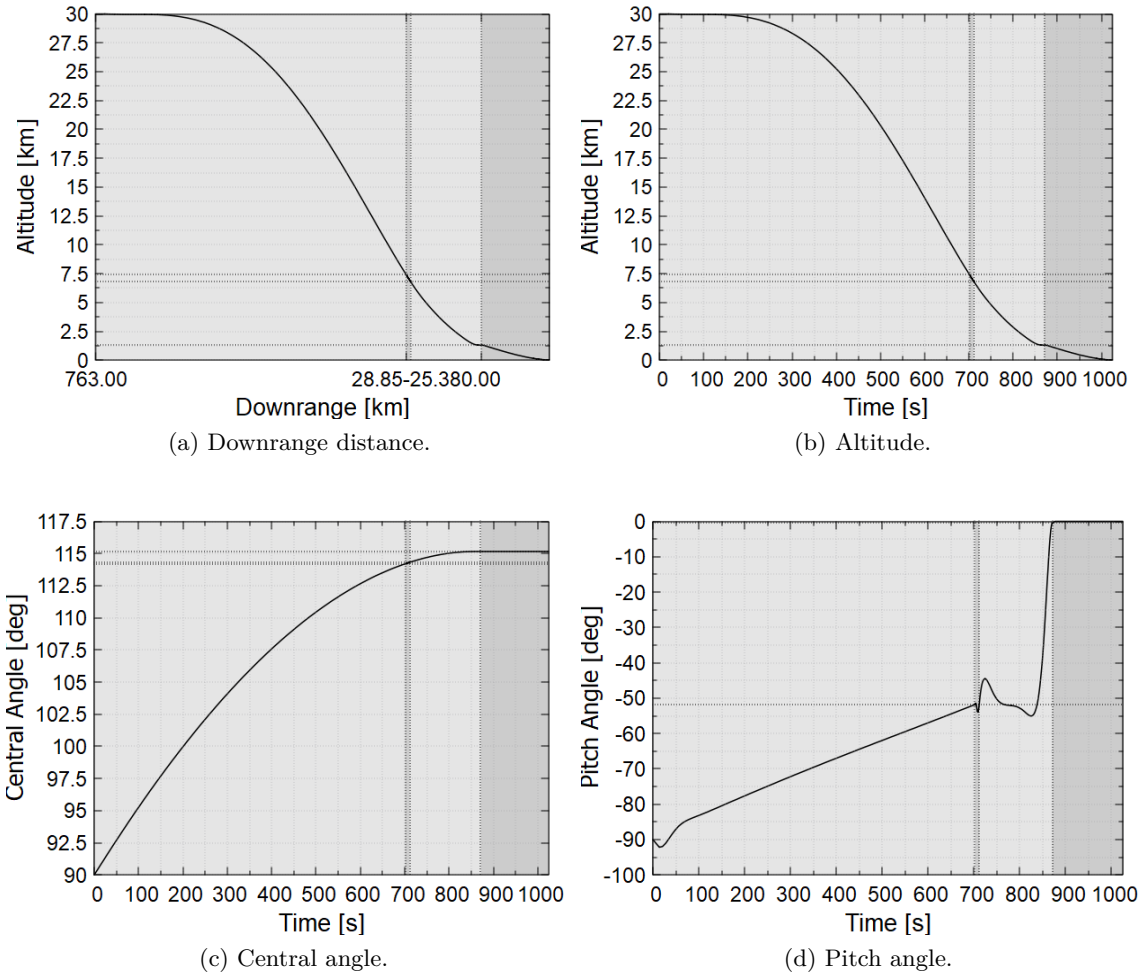


Figure 4.4: The optimal descent trajectory profile over time (Part 1).

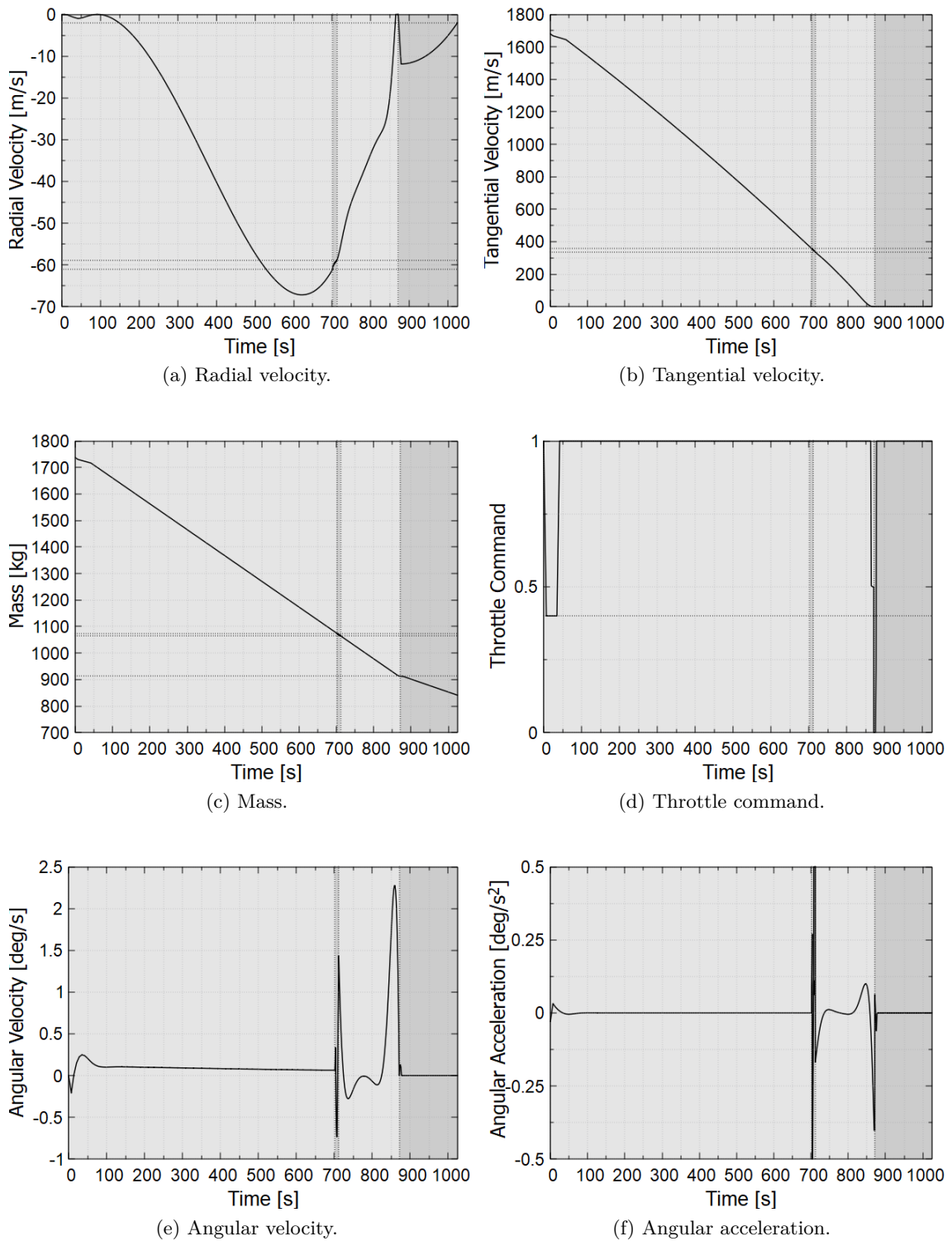


Figure 4.5: The optimal descent trajectory profile over time (Part 2).

# Chapter 5

# Design and Implementation of Visualisation Environment

A visualisation application was developed to simplify the depiction of the computed optimal descent trajectory. This chapter details the design and implementation of the 3D program. Additionally, one can gain an understanding of the tools and methods utilised during the creation process of this application.

## 5.1 Application Design

### Motivation

The goal of this program is to furnish users with a user-friendly tool for visualising the descent trajectory. Derived from the computed optimal trajectory in Chapter 4, the coordinates are used for accurate representation. The application aims to be accessible and easy to understand for all users. It will showcase the Moon and the Chandrayaan-3 spacecraft in a 3D environment. Users can watch an animation of the spacecraft's journey from start to finish and interact with it, adjusting the speed or jumping to different time points. Besides, the application's adaptable design allows for effortless integration of future updates and enhancements, enabling expansion of its capabilities in subsequent versions.

### Application Layout

Upon starting the application, users are greeted with a visualisation screen featuring 3D models of the Moon and the Chandrayaan-3 spacecraft. These models are scaled to maintain proportionality; however, due to Godot's limitations with decimal precision at higher values, the sizes of both the Moon and spacecraft have been adjusted. Originally, the scale ratio of the lunar radius to the spacecraft was 1 738 100:2, but it has been modified to 21 726:0.5, making the Moon 80 times smaller and the spacecraft 4 times smaller than initially intended.

By default, the animation runs in real time and the state variable information, excluding angular velocity, is displayed in the bottom left corner to provide insight into the current status of the descent. The user interface incorporates buttons that allow users to pause or resume the visualisation, as well as adjust the time flow to move forward or backward. A button in the top-left corner lets users restart the animation from the starting position with the initial camera rotation. The slider enables users to jump to different points in time, while the drop-down menu in the top-right corner allows them to alter the animation speed

to 2x, 5x, 10x, 25x or 50x. Additionally, users can change the camera view angle by dragging the right mouse button. In the bottom right corner, an icon with power-off symbol permits users to exit the application at any time during the visualisation. Application screen is illustrated in Figure 5.1.



Figure 5.1: Application Frontend.

## 5.2 Application Implementation

The application was crafted using the open-source 3D engine Godot, selected for its versatile 2D and 3D capabilities, user-friendly interface and support for multiple programming languages. Moreover, as a non-proprietary and open-source, it offers a considerable amount of freedom and flexibility. The trajectory is built within the application and then smoothed out by Bézier curve algorithm. Once ready, the final trajectory, along with the Moon and LL, is shown in a space environment.

### Godot Engine

Godot Engine is a feature-packed, open-source game engine, released under the permissive MIT license, offering comprehensive tools for creating both 2D and 3D games through a unified interface. Furthermore, it is cross-platform, which implies compatibility on various operating systems or devices. Therefore all games can be effortlessly exported to several platforms, including the most common desktop platforms (Windows, macOS, Linux), mobile platforms (Android, iOS), web-based platforms and consoles. It has an all-embracing suite of tools, from robust physics simulation to extensive customisation through plugins and extensions [30]. The officially supported programming languages for Godot are GDScript (an integrated scripting language native to Godot), C# and C++. For this application, the chosen language is: GDScript.

The Godot Engine revolves around two fundamental concepts: nodes and scenes. Nodes serve as the units of functionality and can be thought of as objects with specific properties and behaviours. They can be organised hierarchically, creating parent-child relationships where child nodes inherit attributes and transformations of their parents.

Scenes in Godot are collections of nodes arranged in a tree structure. This enables developers to group nodes together into complex objects, such as a game character or an entire level, which can then be instantiated and reused throughout the project. This design approach simplifies the process of structuring and managing game objects [30].

## Implementation Details

The application is comprised of three scenes: `Space`, `ui_overlay` and `vikram`. Various assets for the main scene have been either sourced or developed. The Moon is represented by a `MeshInstance3D` sphere and is textured with imagery derived from [4]. The space environment is managed by `WorldEnvironment`, which generates a panoramic texture that envelops the entire scene, sourced from [54].

The `Trajectory` is created using the `Path3D` and `PathFollow3D` nodes. The `PathFollow3D` node, which is a child of `Path3D`, calculates the coordinates of a point along the path based on its distance from the initial vertex [30]. Adjusting the offset of the `PathFollow3D` node animates the movement of the Lander. The LL itself is modelled as a `MeshInstance3D` and is referred to as `Vikram` in the application. The `Path3D` node contains a `Curve3D`, which represents a Bézier curve in 3D space [30].

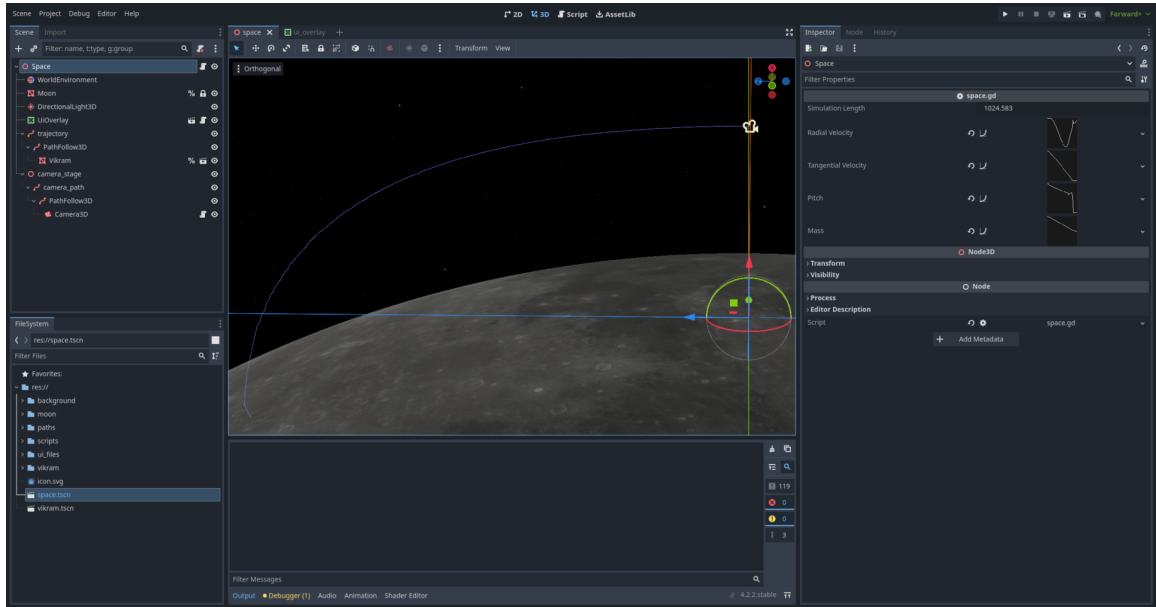


Figure 5.2: Application Design in Godot.

Modifications to the trajectory are necessary due to the imprecision in Godot's rotation handling at higher decimal places. The `camera_stage`, a `Camera3D` node, shows the view from its current position [30]. Last but not least, the `UiOverlay` and its `ui_overlay` scene are responsible for the user interface. This includes pre-loaded state variable information about the spacecraft throughout lunar descent, such as vertical and horizontal velocity,

pitch and mass, which are displayed as time-based curves. Figure 5.2 portrays the program during its development phase.

## Bézier Curve Algorithm

Upon program launch, if the provided trajectory of the LL lacks a sufficient number of points, it might not meet our expectations adequately. This could lead to users observing a bumpy appearance in the displayed trajectory, especially in areas where abrupt changes in direction occur. Recognising the importance of a smooth and seamless visualisation experience, our solution involves employing the Bézier curve algorithm to refine the input trajectory. This algorithm is well-known for its ability to interpolate between control points, thus making the trajectory look more even. By leveraging the Bézier curve algorithm, we ensure that the trajectory transitions fluidly between points.

Scientific computing often necessitates creating lines that traverse predetermined control points, known as knots. Mesh generation serves as a prime example. Even with mesh-free methods, establishing problem boundaries remains vital, typically achieved through boundary splines. These splines consist of polygonal segments, ranging from linear to higher-order polynomials [2]. The cubic Bézier curve can be represented by Equation 5.1 and can be restated as Equation 5.2.

$$\mathbf{B}(t) = (1-t)^3 \mathbf{P}_0 + 3(1-t)^2 t \mathbf{P}_1 + 3(t-1)t^2 \mathbf{P}_2 + t^3 \mathbf{P}_3, \quad t \in [0, 1] \quad (5.1)$$

$$\mathbf{B}(t) = (1-t)^3 \mathbf{P}_0 + 3(t-2t^2+t^3) \mathbf{P}_1 + 3(t^2-t^3) \mathbf{P}_2 + t^3 \mathbf{P}_3 \quad (5.2)$$

Within this definition, the endpoints (knots) are denoted by points  $\mathbf{P}_0$  and  $\mathbf{P}_3$ , while the remaining two points function as control points, shaping the curve. It is worth noting that the curve generally does not intersect these points. Our goal is to guarantee continuity in both the first and second derivatives across the spline boundary. This requirement yields two equations, one for each derivative, at each spline interface. These equations are then utilised to determine the control points. The first and second derivatives are expressed in Equations 5.3 and 5.4.

$$\mathbf{B}'(t) = -3(1-t)^2 \mathbf{P}_0 + 3(1-4t+3t^2) \mathbf{P}_1 + 3(2t-3t^2) \mathbf{P}_2 + 3t^2 \mathbf{P}_3 \quad (5.3)$$

$$\mathbf{B}''(t) = 6(1-t) \mathbf{P}_0 + 3(-4+6t) \mathbf{P}_1 + 3(2-6t) \mathbf{P}_2 + 6t \mathbf{P}_3 \quad (5.4)$$

For both derivatives, the conditions at the left boundary of the “*i*-th” segment are given by Equations 5.5 and 5.6.

$$\mathbf{B}'_i(0) = \mathbf{B}'_{i-1}(1) \quad (5.5)$$

$$\mathbf{B}''_i(0) = \mathbf{B}''_{i-1}(1) \quad (5.6)$$

Considering the curve’s continuity, we find that  $\mathbf{P}_{0,i} = \mathbf{P}_{3,i-1} = \mathbf{K}_i$ , the “*i*-th” knot point. Consequently, we can remove the complexities from the above equations and get Equations 5.7 and 5.8.

$$2\mathbf{K}_i = \mathbf{P}_{1,i} + \mathbf{P}_{2,i-1} \quad (5.7)$$

$$-2\mathbf{P}_{1,i} + \mathbf{P}_{2,i} = \mathbf{P}_{1,i-1} - 2\mathbf{P}_{2,i-1} \quad (5.8)$$

At the internal knots, where two segments meet, Equations 5.9 and 5.10 are defined. From a mathematical perspective, this implies that we have  $2(n-1)$  equations for  $2n$  unknowns.

To complete the system, we impose two additional natural boundary conditions:  $\mathbf{B}_0''(0) = 0$  and  $\mathbf{B}_{n-1}''(1) = 0$ , indicating that the spline becomes linear at the endpoints.

$$\mathbf{K}_0 - 2\mathbf{P}_{1,0} + \mathbf{P}_{2,0} = 0 \quad (5.9)$$

$$\mathbf{P}_{1,n-1} - 2\mathbf{P}_{2,n-1} + \mathbf{K}_n = 0 \quad (5.10)$$

Figure 5.3 illustrates a representation of a Bézier curve.

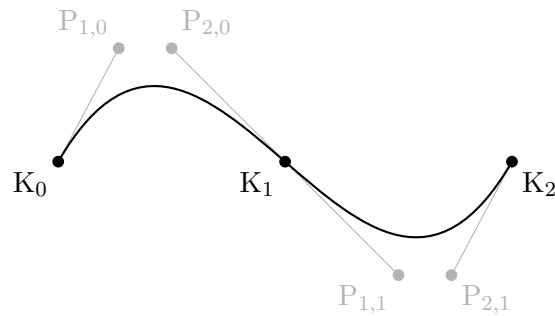


Figure 5.3: Bézier curve with knots and control points.

# Chapter 6

## Results and Potential Improvements

This chapter begins with an evaluation of the optimal descent trajectory, followed by a comparison with the actual trajectory observed during the Chandrayaan-3 mission. Moreover, it delves into suggestions for potential improvements in both the optimisation process and the visualisation application.

### Comparison of Descent Trajectories

The feasibility of the computed optimal descent trajectory satisfies all proposed criteria, affirming its success. The most effective approach to validate the accuracy of the numerical model is through a comparison with either the planned trajectory of the Chandrayaan-3 mission or real flight data. Unfortunately, there is no official data on the intended path of the mission and although real flight data exists, it is only partially comparable. The actual descent trajectory was reconstructed by sampling images, such as the one depicted in the picture [55]. According to these observations, the powered descent commences at an altitude of 30 km above the lunar surface, aligning closely with the starting point of the optimised descent trajectory. The four phases of the optimal descent trajectory are individually evaluated, utilising a diligent verification method for each phase. To provide the best possible comparison, the figure in Section 2.4 is selected due to its close resemblance the the power descent depicted in the live video broadcasts on News18 Kannada's channel [48].

The *Rough Braking Phase* was intended to reduce the altitude from 30 km to 7.4 km and achieve target vertical and horizontal velocities of  $-61 \text{ m s}^{-1}$  and  $358 \text{ m s}^{-1}$ , in this order. It was expected to last approximately 690 s and cover 713.5 km downrange distance. In comparison, the obtained results were a duration of 701.538 s and a distance of 734.145 km. The difference of only 10 s indicates reasonable data consistency. Additionally, the slight adjustment in the spacecraft's pitch angle by  $38.140^\circ$  further enhances the potential accuracy of the trajectory.

During the *Attitude Hold Phase*, it was crucial to maintain the existing pitch angle without deviation. The goal was to decrease radial and tangential velocities by  $2 \text{ m s}^{-1}$  and  $22 \text{ m s}^{-1}$ , respectively, within a planned time frame of 10 s. The achieved results demonstrate that the spacecraft's pitch angle remained consistent at both the start and the end

of the phase and the velocities were diminished to the desired values within 10.061 s. This performance indicates a lack of errors in this phase.

The *Fine Braking Phase* was designed to lower the height from 6.8 km above the ground to either 800 m or 1 300 m, with the chosen altitude being 1 300 m as discussed in Section 2.4. The phase aimed to nullify both vertical and horizontal speeds. Moreover, the angular velocity was brought to zero to enable a smooth and controlled descent. The spacecraft was oriented in a fully vertical position, maintaining a pitch angle of 0°. These objectives were achieved within 159.446 s, covering a downrange distance of 25.376 km. This compares favourably to the anticipated duration of 175 s and distance of 28.52 km.

Lastly, throughout the *Terminal Descent Phase*, the spacecraft was meant to safely touchdown with the greatest possible fuel capacity. The final radial velocity should not exceed 2 m s<sup>-1</sup> and the tangential should not be higher than 0.5 m s<sup>-1</sup>. To secure a soft landing in vertical legs-down position, the pitch angle of the vehicle was preferred to be within the range of -0.5° to 0.5° and the angular velocity was desired to be zero. These conditions were met within 159.450 s, covering 0 km across the surface, compared to the planned 213 s (without hovering or retargeting) and a maximum distance of 150 m travelled.

The computed optimal descent trajectory lasted for 1 024.583 s and covered a downrange distance of 762.998 km. The spacecraft's weight at touchdown was 840.766 kg, with an excess of 133.286 kg of unused fuel. In comparison, the actual observed trajectory took 1 088 s, travelled 745.5 km and soft-landed with mass of 771 kg, having an approximate surplus of 64 kg of unburnt fuel, as mentioned in [47]. Thus, the presented solution appears to be optimal, as it was in our best interest to maintain the trajectory's credibility.

## Further Improvements

In this thesis, enhancing the descent trajectory could be achieved by incorporating all six degrees of motion and comparing the optimal path with the mission plan, assuming it becomes available in the future. This approach would enable for a more realistic simulation of the descent manoeuvre. However, this was not implemented in the current version due to the incomplete data. Further improvements could include optimising a longer trajectory, such as from the deorbit phase or even from Earth, as well as integrating trajectory or state variable curves from datasets while preserving the original scale.

The application would greatly benefit from including an accurate topological map of the lunar surface, which could differentiate between mountains, craters and specific landing site. Such detailed mapping would enable more precise touchdown positioning and elevate the overall realism of the simulation. Additionally, incorporating a flame animation to the spacecraft during thrust would further improve the visual authenticity.

# Chapter 7

## Conclusion

The aim of this bachelor thesis encompassed two main objectives: computing the optimal lunar descent trajectory for the Chandrayaan-3 spacecraft and creating a simulation of it in a 3D environment. Both of them were successfully accomplished.

The optimised descent trajectory reaches all essential requirements, effectively mitigating risks that could potentially compromise mission success and ensuring a soft landing for the Chandrayaan-3 spacecraft. Spanning approximately 1 024.583 s, the manoeuvre conserves 133.286 kg (12.946 %) of fuel. Despite evaluating several alternative trajectories, none proved superior in efficacy.

The initial steps involved delving into the history of the Chandrayaan-3 mission and extracting crucial data, including detailed trajectory descriptions and LL's technical parameters. With this foundational information, the next phase entailed deriving the EOMs to position the LL within a coordinate system, laying the groundwork for tackling the optimisation problem. Following that, optimisation theory was studied and the optimal descent trajectory was modelled as an OCP using specialised software Bocop, known for its proficiency in such tasks. After implementing the problem in Bocop's environment and documenting the results, the third phase of the project unfolded. In this subsequent phase, attention shifted towards visualising the descent manoeuvre using the 3D engine Godot. This involved crafting the input format for the application, parsing the dataset and generating a 3D animation to provide an intuitive trajectory visualisation, enabling users to swiftly comprehend computed lunar descent paths. Finally, the optimal and actual descent trajectories were compared, leading to a comprehensive assessment of the project's outcomes.

Potential enhancements could involve calculating the optimal descent trajectory in six degrees of freedom or extending the length of the computed trajectory. Furthermore, the visualisation environment could might be improved by including a more detailed map of Moon's surface or by adding a flame animation to the vehicle.

# Bibliography

- [1] BONNANS, F., MARTINON, P., GIORGI, D., GRÉLARD, V., MAINDRAULT, S. et al. *BOCOP 2.2.0 - User Guide* [online]. 2019 [cit. 2024-01-10]. Available at: <https://files.inria.fr/bocop/UserGuide-BOCOP.pdf>.
- [2] BRIEDA, L. *Smooth Bézier Spline Through Prescribed Points* [online]. 17. June 2012 [cit. 2024-04-02]. Available at: <https://www.particleincell.com/2012/bezier-splines/>.
- [3] BRÜGGE, N. *SPACE LAUNCH VEHICLES* [online]. [cit. 2024-03-15]. Available at: [https://www.b14643.de/Spacerockets\\_1/India/India.htm](https://www.b14643.de/Spacerockets_1/India/India.htm).
- [4] CGT3D. *8K Photo Realistic Moon* [online]. 07. September 2020 [cit. 2024-05-10]. Available at: <https://www.cgtrader.com/free-3d-models/space/planet/8k-photo-realistic-moon>.
- [5] COLASURDO, G. *Astrodynamicics* [online]. Polytechnic University of Turin, 2006 [cit. 2024-01-02]. Available at: [http://dma.ing.uniroma1.it/users/lss\\_mo/MATERIALE/AvanziniColasurdoAstrodynamics.pdf](http://dma.ing.uniroma1.it/users/lss_mo/MATERIALE/AvanziniColasurdoAstrodynamics.pdf).
- [6] DARTMOUTH, M. *The First and Second Derivatives* [online]. [cit. 2024-02-29]. Available at: <https://math.dartmouth.edu/opencalc2/cole/lecture8.pdf>.
- [7] EOPORTAL. *Chandrayaan-3* [online]. 14. March 2024 [cit. 2024-03-10]. Available at: <https://www.eoportal.org/satellite-missions/chandrayaan-3#references>.
- [8] FAJMON, B., HLAVIČKOVÁ, I., NOVÁK, M. and VÍTOVEC, J. *Numerická matematika a pravděpodobnost*. 2014 [cit. 2024-01-10]. Available at: <https://www.vut.cz/studenti/predmety/detail/174531?apid=174531>.
- [9] FOLKNER, W. M., WILLIAMS, J. G. and BOGGS, D. H. *The Planetary and Lunar Ephemeris DE 421* [online]. 2009 [cit. 2024-01-15]. Available at: [https://ipnpr.jpl.nasa.gov/progress\\_report/42-178/178C.pdf](https://ipnpr.jpl.nasa.gov/progress_report/42-178/178C.pdf).
- [10] FRASER, U. S. *5.8 Optimization Problems* [online]. [cit. 2024-02-25]. Available at: [https://www.sfu.ca/math-coursenotes/Math%20157%20Course%20Notes/sec\\_Optimization.html](https://www.sfu.ca/math-coursenotes/Math%20157%20Course%20Notes/sec_Optimization.html).
- [11] GHOSH, M. K. *Optimal Control Theory* [online]. [cit. 2024-02-29]. Available at: [https://www.iisertvm.ac.in/files/get\\_file/4c27cea8526af8cfee3be5e183ac9605](https://www.iisertvm.ac.in/files/get_file/4c27cea8526af8cfee3be5e183ac9605).
- [12] HAWKINS, A. M. *Constrained trajectory optimization of a soft lunar landing from a parking orbit*. Cambridge, 2005. Masters Thesis. Massachusetts Institute of Technology. Dept. of Aeronautics and Astronautics. Available at: <https://dspace.mit.edu/handle/1721.1/32431>.

- [13] INDIA, T. T. of. Chandrayaan-3 launch delayed further to 2022. *The Times of India*. February 2021, [cit. 2024-02-20]. Available at: <https://timesofindia.indiatimes.com/india/chandrayaan-3-launch-delayed-further-to-2022/articleshow/81136400.cms>.
- [14] ISRO. *Chandrayaan-1* [online]. [cit. 2024-02-20]. Available at: [https://www.isro.gov.in/Chandrayaan\\_1.html](https://www.isro.gov.in/Chandrayaan_1.html).
- [15] ISRO. *Chandrayaan-2* [online]. [cit. 2024-02-16]. Available at: [https://www.isro.gov.in/Chandrayaan2\\_science.html](https://www.isro.gov.in/Chandrayaan2_science.html).
- [16] ISRO. *Chandrayaan-2 FAQ* [online]. [cit. 2024-02-20]. Available at: <https://web.archive.org/web/20190629122319/https://www.isro.gov.in/chandrayaan2-faq>.
- [17] ISRO. *Chandrayaan-3* [online]. [cit. 2024-02-20]. Available at: [https://www.isro.gov.in/Chandrayaan3\\_Details.html](https://www.isro.gov.in/Chandrayaan3_Details.html).
- [18] ISRO. *Chandrayaan2* [online]. [cit. 2024-02-20]. Available at: [https://www.isro.gov.in/Chandrayaan\\_2.html](https://www.isro.gov.in/Chandrayaan_2.html).
- [19] ISRO. *CHANDRAYAN2* [online]. [cit. 2024-02-16]. Available at: <https://www.isro.gov.in/Launcher.html>.
- [20] ISRO. *LVM3(Geosynchronous Satellite Launch Vehicle Mk III)* [online]. [cit. 2024-03-01]. Available at: [https://www.isro.gov.in/GSLVmk3\\_CON.html](https://www.isro.gov.in/GSLVmk3_CON.html).
- [21] ISRO. *LVM3 S200 BOOSTER FIRST STATIC TEST (S200-ST-01)* [online]. 24. January 2010 [cit. 2024-03-15]. Available at: [https://web.archive.org/web/20130311191452/http://isro.org/pressrelease/contents/2010/pdf/S200\\_STATIC\\_TEST-01.pdf](https://web.archive.org/web/20130311191452/http://isro.org/pressrelease/contents/2010/pdf/S200_STATIC_TEST-01.pdf).
- [22] ISRO. *Chandrayaan-3 Mission update 07.15.2023* [online]. 15. July 2023 [cit. 2024-03-05]. Available at: <https://twitter.com/isro/status/1680239822110162944>.
- [23] ISRO. *Chandrayaan-3 Mission update 08.01.2023* [online]. 1. August 2023 [cit. 2024-03-05]. Available at: <https://twitter.com/isro/status/1686327939280035840>.
- [24] ISRO. *Chandrayaan-3 Mission update 08.16.2023* [online]. 16. August 2023 [cit. 2024-03-05]. Available at: <https://twitter.com/isro/status/1691655268449603770>.
- [25] ISRO. *Chandrayaan-3 Mission update 08.20.2023* [online]. 20. August 2023 [cit. 2024-03-05]. Available at: <https://twitter.com/isro/status/1692995757413192015>.
- [26] ISRO. *Returns to home Earth: Chandrayaan-3 Propulsion Module moved from Lunar orbit to Earth's orbit* [online]. 04. December 2023 [cit. 2024-03-10]. Available at: [https://www.isro.gov.in/Ch3\\_Propulsion\\_Module\\_moved\\_from\\_Lunar\\_orbit\\_to\\_Earth\\_orbit.html](https://www.isro.gov.in/Ch3_Propulsion_Module_moved_from_Lunar_orbit_to_Earth_orbit.html).
- [27] JOHNSON, T. A. ‘15 minutes of terror’: What should happen in the final minutes of Chandrayaan-3 lander’s descent on the Moon. *The Indian Express*. August 2023, [cit. 2024-05-01]. Available at: <https://indianexpress.com/article/explained/explained-sci-tech/chandrayaan-3-lander-descent-phases-8902275/>.

- [28] JOSHI, S. *ISRO successfully tests world's 3rd largest solid booster* [online]. 13. April 2018 [cit. 2024-03-01]. Available at: [https://www.dnaindia.com/technology/report\\_isro-successfully-tests-world-s-3rd-largest-solid-booster\\_1338945](https://www.dnaindia.com/technology/report_isro-successfully-tests-world-s-3rd-largest-solid-booster_1338945).
- [29] LAMBERS, J. *Maximum and Minimum Values* [online]. 2009 [cit. 2024-02-29]. Available at: <https://www.math.sci.hokudai.ac.jp/~s.settepanella/teachingfile/Calculus/Calculus1/pagine/lecture8.pdf>.
- [30] LINIETSKY, J. and MANZUR, A. *Godot Engine 4.2 documentation* [online]. [cit. 2024-03-20]. Available at: <https://docs.godotengine.org/en/stable/index.html>.
- [31] MADANAPALLE, A. Here is Exactly What Chandrayaan-3 Lander Will Do During Powered Descent to Surface of Moon. *News9 Live*. August 2023, [cit. 2024-05-01]. Available at: <https://www.news9live.com/science/here-is-exactly-what-chandrayaan-3-lander-will-do-during-powered-descent-to-surface-of-moon-2260048>.
- [32] MATHAVARAJ, S., NEGI, K. and VAIBHAV, G. *ISRO's Unprecedented Journey to the Moon* [online]. 2020 [cit. 2024-03-22]. Available at: <https://www.sciencedirect.com/science/article/pii/S0094576520304732>.
- [33] MEHTA, J. Chandrayaan-3 Makes Historic Touchdown on the Moon. *Scientific American*. August 2023, [cit. 2024-01-10]. Available at: <https://www.scientificamerican.com/article/chandrayaan-3-makes-historic-touchdown-on-the-moon/>.
- [34] MERRIAM WEBSTER, D. *Moon landing* [online]. [cit. 2024-03-24]. Available at: <https://www.merriam-webster.com/dictionary/moon%20landing>.
- [35] MORRIS, D. *Introduction to Optimization: Theory* [online]. 20. february 2020 [cit. 2024-02-25]. Available at: <https://www.tangramvision.com/blog/introduction-to-optimization-theory>.
- [36] NASA. *Chandrayaan-1 / Moon Impact Probe* [online]. [cit. 2024-02-16]. Available at: <https://science.nasa.gov/mission/chandrayaan-1/>.
- [37] NASA. *Chandrayaan 2* [online]. [cit. 2024-02-16]. Available at: <https://nssdc.gsfc.nasa.gov/nmc/spacecraft/display.action?id=2019-042A>.
- [38] NASA. *Chandrayaan 3* [online]. [cit. 2024-01-15]. Available at: <https://nssdc.gsfc.nasa.gov/nmc/spacecraft/display.action?id=2023-098A>.
- [39] NASA. *Luna 9* [online]. [cit. 2024-03-24]. Available at: <https://nssdc.gsfc.nasa.gov/nmc/spacecraft/display.action?id=1966-006A>.
- [40] NASA. *Moon Fact Sheet* [online]. [cit. 2024-01-15]. Available at: <https://nssdc.gsfc.nasa.gov/planetary/factsheet/moonfact.html>.
- [41] NASA. *Newton's Laws of Motion* [online]. [cit. 2024-03-24]. Available at: <https://www1.grc.nasa.gov/beginners-guide-to-aeronautics/newtons-laws-of-motion/>.
- [42] NASA. *The Lunar Landing Research Vehicle*. NASA SP-2004-4535. NASA, 2005 [cit. 2024-03-24]. Available at: [https://www.nasa.gov/wp-content/uploads/static/history/alsj/LLRV\\_Monograph.pdf](https://www.nasa.gov/wp-content/uploads/static/history/alsj/LLRV_Monograph.pdf).

- [43] NASA. *Full Moon* [online]. 2017 [cit. 2024-03-01]. Available at: [https://images.nasa.gov/details-GSFC\\_20171208\\_Archive\\_e001861](https://images.nasa.gov/details-GSFC_20171208_Archive_e001861).
- [44] NASA. What is Artemis? *NASA General*. July 2019, [cit. 2024-05-12]. Available at: <https://www.nasa.gov/general/what-is-artemis/>.
- [45] NASA. Artemis. *NASA Humans in Space*. 2024, [cit. 2024-05-12]. Available at: <https://www.nasa.gov/humans-in-space/artemis/>.
- [46] NASA EARTH OBSERVATORY. *Dust Traverses the Atlantic Ocean* [online]. 2020 [cit. 2024-03-01]. Available at: <https://earthobservatory.nasa.gov/images/146871/dust-traverses-the-atlantic-ocean?src=ve>.
- [47] NDTV. *Chandrayaan 3 / Meet India's Moon Stars: Shiv, Shakti and Nataraj* [online]. 28. September 2023 [cit. 2024-05-02]. Available at: <https://www.youtube.com/watch?v=QtsCwdsKOXM>.
- [48] NEWS18 KANNADA. *LIVE: Chandrayaan 3 India's Moon Exploration / Prof S Pradeep Memorial Lecture / S Somanath / IISc* [online]. 5. August 2023 [cit. 2024-03-22]. Available at: [https://www.youtube.com/watch?v=fZ2sNRP1opY&ab\\_channel=News18Kannada](https://www.youtube.com/watch?v=fZ2sNRP1opY&ab_channel=News18Kannada).
- [49] OHSIN. *Chandrayaan-3: 'Vikram' Landing Attempt Updates and Discussion*. [online]. 2023 [cit. 2024-03-20]. Available at: [https://www.reddit.com/r/ISRO/comments/15waz81/chandrayaan3\\_vikram\\_landing\\_attempt\\_updates\\_and/](https://www.reddit.com/r/ISRO/comments/15waz81/chandrayaan3_vikram_landing_attempt_updates_and/).
- [50] SOLIDBOOSTERS. *Direct Trans-Lunar injection(TLI) payloads capacity of GSLV Mk-3 is around 3000 kg.* [online]. 22. February 2024 [cit. 2024-03-01]. Available at: <https://x.com/SolidBoosters/status/1760551812216787202>.
- [51] STOVER, C. and WEISSTEIN, E. *Cartesian Coordinates* [online]. From MathWorld—A Wolfram Web Resource [cit. 2024-01-02]. Available at: <https://mathworld.wolfram.com/CartesianCoordinates.html>.
- [52] STOVER, C. and WEISSTEIN, E. *Polar Coordinates* [online]. From MathWorld—A Wolfram Web Resource [cit. 2024-01-02]. Available at: <https://mathworld.wolfram.com/PolarCoordinates.html>.
- [53] THOMAS WILLIAMS, R. L. D. K. J. C. G. E. A. W. *Gnuplot homepage* [online]. May 2024 [cit. 2024-05-03]. Available at: <http://www.gnuplot.info/>.
- [54] TYRO. *3D Space Simulation Tool* [online]. [cit. 2024-05-10]. Available at: <https://tools.wwtyro.net/space-3d/index.html#animationSpeed=1&fov=80&nebulae=false&pointStars=true&resolution=4096&seed=3hiv0tgq36a0&stars=true&sun=true>.
- [55] WIKIPEDIA. *File: Chandrayaan-3 Lander Powered Descent Profile.svg* [online]. 8. August 2023 [cit. 2024-03-22]. Available at: [https://commons.wikimedia.org/wiki/File:Chandrayaan-3\\_Lander\\_Powered\\_Descent\\_Profile.svg](https://commons.wikimedia.org/wiki/File:Chandrayaan-3_Lander_Powered_Descent_Profile.svg).

## Appendix A

# Astronomical Bodies and Launch Vehicle in Chandrayaan-3 Mission

### The Earth



Figure A.1: The Earth.  
Source: [46].

Equatorial radius	6 378.137 km
Mass	$5.972\ 4 \times 10^{24}$ kg
Gravitational parameter	$3.986\ 004\ 362\ 33 \times 10^{14}$ m $^3$ s $^{-2}$
Surface gravity	9.80 m s $^{-2}$
Escape velocity	11.2 km s $^{-1}$
Atmospheric pressure	1 bar

Table A.1: Earth specifications. Source: [9, 40].

### The Moon



Figure A.2: The Moon.  
Source: [43].

Equatorial radius	1 738.1 km
Mass	$0.073\ 46 \times 10^{24}$ kg
Gravitational parameter	$4.902\ 800\ 076 \times 10^{12}$ m $^3$ s $^{-2}$
Surface gravity	1.62 m s $^{-2}$
Escape velocity	2.38 km s $^{-1}$
Atmospheric pressure	$3 \times 10^{-15}$ bar (vacuum)
Mean orbital radius	378 000 km
Mean orbital velocity	1.022 km s $^{-1}$

Table A.2: Moon specifications. Source: [9, 40].

## LVM3-M4



Figure A.3: LVM3-M4 rocket.  
Source: [20].

Manufacturer	ISRO
Height	43.5 m
Diameter	4 m
Weight (fuelled)	640 000 kg
Payload mass	3 895 kg
Stages	3
Propellant	HTPB (Solid) UH <sub>25</sub> + N <sub>2</sub> O <sub>4</sub> (Liquid) LH <sub>2</sub> & LOX (Cryo)
Propulsion (1 <sup>st</sup> stage)	2 S200s
Propulsion (2 <sup>nd</sup> stage)	2 Vikas engines
Propulsion (3 <sup>rd</sup> stage)	1 CE-20
Thrust (1 <sup>st</sup> stage)	5 150 kN
Thrust (2 <sup>nd</sup> stage)	1 598 kN
Thrust (3 <sup>rd</sup> stage)	186.36 kN
Payload to LEO	8 000 kg
Payload to GTO	4 000 kg
Payload to TLI	3 000 kg

Table A.3: LVM3-M4 specifications. Source: [20, 50].

# Appendix B

## Additional Specifications

Table B.1: S200 technical specifications. Source: [20, 21, 50].

Manufacturer	Vikram Sarabhai Space Centre
Propellant	206.7 t of Solid-HTPB-based
Maximum Sea Level (SL) thrust	4 942.5 kN
SL $I_{sp}$	227 s (2 226 m s <sup>-1</sup> )
Burn time	128.6 s
Diameter	3.2 m

Table B.2: Vikas engine technical specifications. Source: [3, 20, 50].

Manufacturer	Godrej & Boyce and MTAR Technologies
Propellant	117.8 t of UDMH + N <sub>2</sub> O <sub>4</sub>
Maximum Sea Level (SL) thrust	1 611.2 kN
SL $I_{sp}$	282.97 s (2 775 m s <sup>-1</sup> )
Burn time	203 s
Diameter	4 m

Table B.3: CE-20 technical specifications. Source: [3, 20, 50].

Manufacturer	Vikram Sarabhai Space Centre
Propellant	28.6 t of LH <sub>2</sub> + LOX
Maximum (vacuum) thrust	189.3 kN
Vac. $I_{sp}$	448.78 s (4 401 m s <sup>-1</sup> )
Burn time	665 s
Diameter	4 m

## Appendix C

# Contents of Associated Media Drive

- `/xdoeri00-BP.pdf`: pdf version of the thesis
- `/thesis.zip`: compressed source files of the thesis
- `/bocop/`: directory containing the source files of the optimisation problem
- `/src/`: directory containing the files of the implemented application